Development of novel cyclic peptides as pro-apoptotic agents

Accepted Manuscript

Development of novel cyclic peptides as pro-apoptotic agents

Margherita Brindisi, Samuele Maramai, Simone Brogi, Emanuela Fanigliulo, Stefania Butini, Egeria Guarino, Alice Casagni, Stefania Lamponi, Claudia Bonechi, Seema M. Nathwani, Federica Finetti, Francesco Ragonese, Paola Arcidiacono, Pietro Campiglia, Salvatore Valenti, Ettore Novellino, Roberta Spaccapelo, Lucia Morbidelli, Daniela M. Zisterer, Clive D. Williams, Alessandro Donati, Cosima Baldari, Giuseppe Campiani, Cristina Ulivieri, Sandra Gemma

PII: S0223-5234(16)30273-2

DOI: 10.1016/j.ejmech.2016.04.001

Reference: EJMECH 8515

To appear in: *European Journal of Medicinal Chemistry*

Received Date: 19 February 2016

Revised Date: 31 March 2016

Accepted Date: 1 April 2016

Please cite this article as: M. Brindisi, S. Maramai, S. Brogi, E. Fanigliulo, S. Butini, E. Guarino, A. Casagni, S. Lamponi, C. Bonechi, S.M. Nathwani, F. Finetti, F. Ragonese, P. Arcidiacono, P. Campiglia, S. Valenti, E. Novellino, R. Spaccapelo, L. Morbidelli, D.M. Zisterer, C.D. Williams, A. Donati, C. Baldari, G. Campiani, C. Ulivieri, S. Gemma, Development of novel cyclic peptides as pro-apoptotic agents, *European Journal of Medicinal Chemistry* (2016), doi: 10.1016/j.ejmech.2016.04.001.

Graphical Abstract

Development of novel cyclic peptides as pro-apoptotic agents

Margherita Brindisi, Samuele Maramai, Simone Brogi, Emanuela Fanigliulo, Stefania Butini,* Egeria Guarino, Alice Casagni, Stefania Lamponi, Claudia Bonechi, Seema M. Nathwani, Federica Finetti, Francesco Ragonese, Paola Arcidiacono, Pietro Campiglia, Salvatore Valenti, Ettore Novellino, Roberta Spaccapelo, Morbidelli Lucia, Daniela M. Zisterer, Clive D. Williams, Alessandro Donati, Cosima Baldari, Giuseppe Campiani,* Cristina Ulivieri, Sandra Gemma.

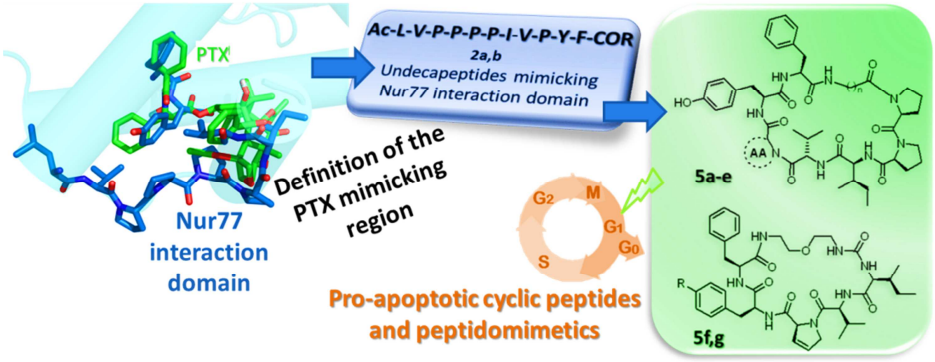

Development of novel cyclic peptides as pro-apoptotic agents

Margherita Brindisi,[1,2] Samuele Maramai,[1,2] Simone Brogi,[1,2] Emanuela Fanigliulo,[3] Stefania Butini,[1,2,*] Egeria Guarino,[1,2] Alice Casagni,[1,2] Stefania Lamponi,[1,2] Claudia Bonechi,[1,2] Seema M. Nathwani,[4] Federica Finetti,[2,3] Francesco Ragonese,[5] Paola Arcidiacono,[5] Pietro Campiglia,[6] Salvatore Valenti,[1,2] Ettore Novellino,[1,7] Roberta Spaccapelo,[5] Lucia Morbidelli,[2,3] Daniela M. Zisterer,[4] Clive D. Williams,[4] Alessandro Donati,[1,2] Cosima Baldari,[3] Giuseppe Campiani,[1,2,**] Cristina Ulivieri,[3] Sandra Gemma.[1,2]

[1]*European Research Centre for Drug Discovery and Development (NatSynDrugs), Siena University, via Aldo Moro 2, I-53100 Siena, Italy*

[2]*Istituto Toscano Tumori, Siena University, via Aldo Moro 2, I-53100 Siena, Italy*

[3]*Department of Life Sciences, via Aldo Moro 2, I-53100 Siena, Italy*

[4]*School of Biochemistry and Immunology, Trinity Biomedical Sciences Institute, Trinity College Dublin, 152-160 Pearse Street, Dublin 2, Ireland*

[5]*Department of Experimental Medicine, Università degli Studi di Perugia, P.le Gambuli, I-06132 Perugia, Italy*

[6]*Dipartimento DIFARMA, Università di Salerno, I-84084 Fisciano, Salerno, Italy*

[7]*Dipartimento di Farmacia, University of Naples Federico II, via D. Montesano 49, I-80131 Naples, Italy*

[*]Corresponding author. Tel.: +39 0577234161; e-mail: butini3@unisi.it

**Corresponding author. Tel.: +39-0577-234172; e-mail: campiani@unisi.it

Keywords: Pro-apoptotic agents; Anticancer agents; Cyclic peptides; Peptidomimetics; Nur77; Tubulin; Bcl-2; NMR studies; Molecular modelling; Confocal microscopy; FACS analysis.

Abbreviations: ADT, AutoDock Tools; COSY, correlation spectroscopy; DBU, 1,8-Diazabicyclo[5.4.0]undec-7-ene; DCM, dichloromethane; DHPro, 3,4-dehydro-(*L*)-proline; DIPEA, *N*,*N*-Diisopropylethylamine; DMEM, Dulbecco's Modified Eagle's medium; DMF, *N*,*N*-dimethylformamide; DMSO, dimethyl sulfoxide; EDCI, 1-Ethyl-3-(3-dimethylaminopropyl)carbodiimide; EEDQ, N-Ethoxycarbonyl-2-ethoxy-1,2-dihydroquinoline; FCS, Fetal Calf Serum; GA, Genetic algorithm; GB/SA, Generalized-Born/Surface-Area; HATU, (1-[Bis(dimethylamino)methylene]-1H-1,2,3-triazolo[4,5-b]pyridinium 3-oxid hexafluorophosphate); HOBt, *N*-Hydroxybenzotriazole; MCMM, Monte Carlo Multiple Minimum; MTAs, microtubule targeting agents; NMR, Nuclear Magnetic Resonance; NOESY, nuclear Overhauser enhancement spectroscopy; OPLS-AA, Optimized Potentials for Liquid Simulations-all atom; PBS, Phosphate-buffered saline; PRCG, Polak-Ribiere conjugate gradient; PTX, paclitaxel; RBL-2H3, rat basophilic leukemia cell line; RIPA, radioimmunoprecipitation assay; TEA, trimethylamine; TFA, trifluoroacetic acid; THF, tetrahydrofuran; TMRM, tetramethylrhodamine methyl ester perchlorate; TOCSY, total correlation spectroscopy.

Abstract

Our recent finding that paclitaxel behaves as a peptidomimetic of the endogenous protein Nur77 inspired the design of two peptides (PEP1 and PEP2) reproducing the effects of paclitaxel on Bcl-2 and tubulin, proving the peptidomimetic nature of paclitaxel. Starting from these peptide-hits, we herein describe the synthesis and the biological investigation of linear and cyclic peptides structurally related

to PEP2. While linear peptides (**2a,b**, **3a,b**, **4**, **6a-f**) were found inactive in cell-based assays, biological analysis revealed a pro-apoptotic effect for most of the cyclic peptides (**5a-g**). Cellular permeability of **5a** (and also of **2a,b**) on HL60 cells was assessed through confocal microscopy analysis. Further cellular studies on a panel of leukemic cell lines (HL60, Jurkat, MEC, EBVB) and solid tumor cell lines (breast cancer MCF-7 cells, human melanoma A375 and 501Mel cells, and murine melanoma B16F1 cells) confirmed the pro-apoptotic effect of the cyclic peptides. Cell cycle analysis revealed that treatment with **5a**, **5c, 5d** or **5f** resulted in an increase in the number of cells in the sub-G_0/G_1 peak. Direct interaction with tubulin (turbidimetric assay) and with microtubules (immunostaining experiments) was assessed *in vitro* for the most promising compounds.

1. Introduction

Microtubules play a key role in mitosis and as such represent an ideal target for anticancer drugs.[1] Compounds able to affect microtubule dynamics are referred to as microtubule targeting agents (MTAs). MTAs, which may bind to different domains both on α- and β-tubulin, are classified as: i) microtubule-depolymerizing agents (e.g. colchicine, nocodazole, vinca alkaloids,[2] and PBOX-compounds[3-6]) and ii) microtubule-polymerizing agents (e.g. taxanes and epothilones).[7] While the mechanism of action of these drugs is well described with respect to their anti-mitotic function, the emerging effects of these compounds on cellular process other than mitosis (apoptosis, chemotaxis, intracellular transport and intracellular signalling) are still under intense investigation.[8] Among MTAs, taxanes are the most important class of antitumor agents and paclitaxel (PTX, **1**, Fig. 1) inhibits microtubule dynamics by interacting with β-tubulin leading to tubulin stabilization, G_2/M cell cycle arrest, and apoptotic cell death.[9] However it is also well known that PTX-induced apoptosis may occur independently from G_2/M arrest.[10] Horwitz and coworkers have indeed demonstrated that **1** at

concentrations lower than that able to induce a G_2/M arrest induces the formation of an aneuploid G_1 cell population.[11] Further, Jordan demonstrated that at low concentrations **1** can block the mitotic process by stabilizing microtubules and not by altering the mass of polymerized microtubules.[12]

Taxanes, besides targeting β-tubulin, also bind to Bcl-2 and behave as Bcl-2 molecular switchers, thus inducing apoptosis.[13] Interestingly, the endogenous orphan nuclear receptor Nur77 (NGFI-B, TR3, NR4A1) also interacts with β-tubulin and Bcl-2 and shares with **1** the same binding site on both proteins.[13] Starting from this evidence, we demonstrated that taxanes mimic β-tubulin and Bcl-2 binding domains of Nur77.[13] To prove the concept two undecapeptides were built, reproducing Nur77 sequences 405-406 and 580-587 linked by a glycine (PEP1) or a proline (PEP2, **2a**, Fig. 1). Biological analysis revealed that PEP2 (**2a**) was slightly more active than PEP1 in mimicking the biological activities of **1** such as tubulin polymerization and opening of the permeability transition pore channel in mitochondria (measured by transmembrane potential evaluated in isolated mitochondria).[13]

Starting from the undecapeptide molecular templates PEP1 and PEP2 (**2a**), we have recently embarked in the development of peptidomimetics mimicking the Nur77 binding domain in order to develop novel pro-apoptotic agents (Table 1). We initially acquired the conformational information on linear undecapeptides in solution by Nuclear Magnetic Resonance (NMR) using **2b** (Fig. 1) as the water soluble counterpart of **2a**. Next, a small series of shorter linear peptides (**3a,b**, **4**, and **6a,e**, Fig. 1 and Table 1) and cyclic peptides (**5a-g**, Fig. 2 and Table 1) were obtained by combining both solid phase and in solution synthesis. Here we have addressed the ability of the newly developed compounds and the reference **2a** to promote apoptosis in different cell lines.

Starting the from the molecular modeling analysis of **1** and **2a,b** with respect of the Nur77 binding domain we investigated the minimum required sequence for activity with the synthesis of shorter linear

peptides **3a,b** (featuring the PTX-superimposable region) and **4** (Fig. 1). The lack of efficacy in cell based assays of these latter analogues prompted the development of cyclic peptides (**5a-g**), with compound **5f** characterized by a relevant reduction of the peptidic nature (Fig. 2 and Table 1).

Cyclic peptides (**5a**, **5c**, **5d** or **5f**), but not the linear peptides or the reference compound **2a**, are able to induce apoptosis in different leukemic cell lines (Jurkat, MEC, and EBV-B) and in solid tumor cell lines (MCF-7, A375, 501Mel, and B16F1). Interaction with tubulin was assessed in vitro by turbidimetric assay and also by immunostaining of microtubules for the most promising compounds. Since confocal microscopy experiments confirmed cell permeability for both the cyclic peptide **5a** and the linear peptide **2a**, we performed mass analysis of cellular lysates for examining the apoptotic effect of **5a** (pro-apoptotic) and **2a** (neither pro-apoptotic, nor cytotoxic).

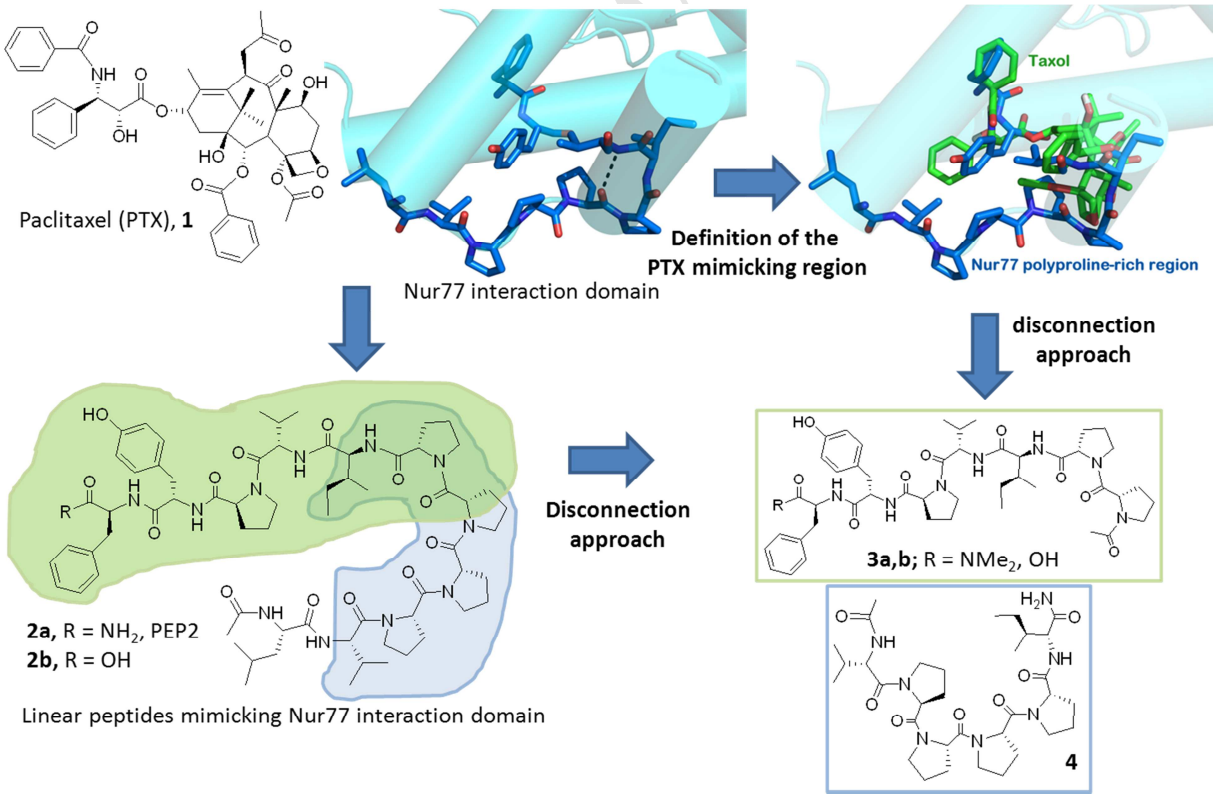

Fig. 1. Reference compounds, paclitaxel, (**1**) and PEP2 (**2a**), and outline of the approach to develop novel PEP2-derivatives **2b**, **3a-b**, and **4**.

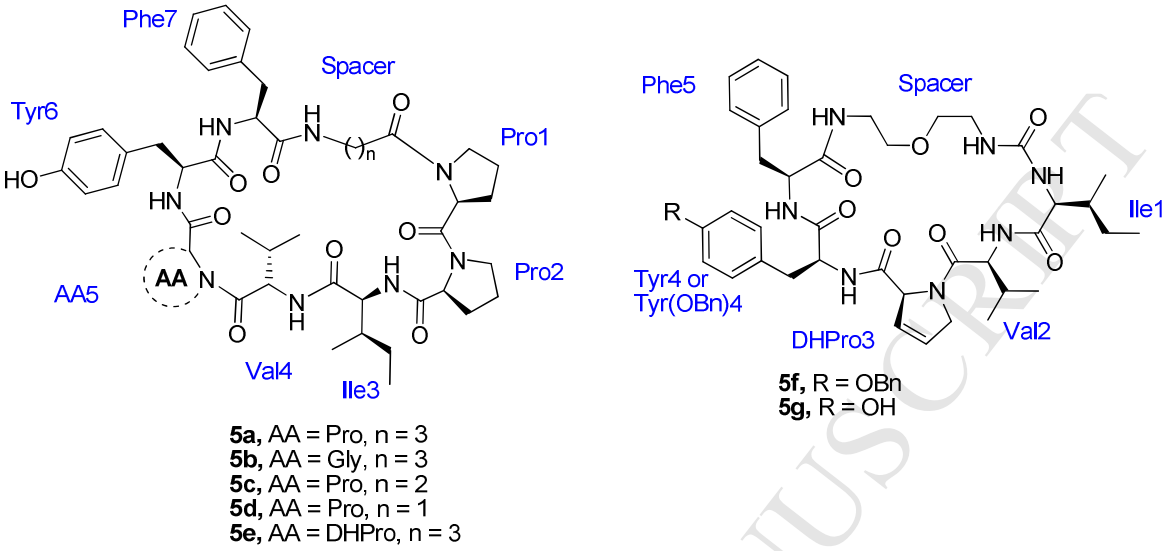

Fig. 2. General structure of the title cyclic peptides **5a-e** and peptidomimetics **5f,g**. (DHPro = 3,4-dehydro-(*L*)-proline).

Table 1. Chemical structure of the developed peptides **2a,b**, **3a,b**, **4**, **5a-g**, **6a-f** and type of synthesis.

Cmpd	Structure	Type of synthesis
2a	Ac-L-V-P-P-P-P-I-V-P-Y-F-$CONH_2$	-
2b	Ac-L-V-P-P-P-P-I-V-P-Y-F-COOH	Solid phase
3a	Ac-P-P-I-V-P-Y-F-$CON(Me)_2$	Solid phase & in solution chemistry
3b	Ac-P-P-I-V-P-Y-F-COOH	Solid phase
4	Ac-V-P-P-P-P-I-$CONH_2$	Solid phase & in solution chemistry
5a	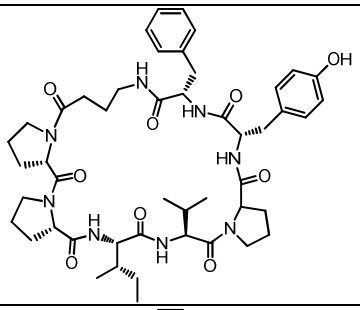	Solid phase & in solution chemistry
5b	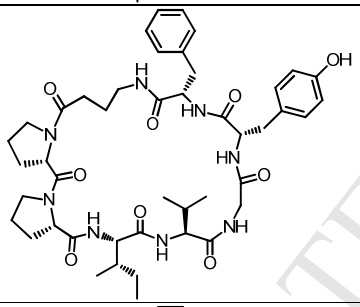	Solid phase & in solution chemistry
5c	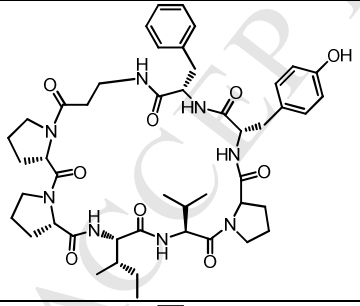	Solid phase & in solution chemistry
5d	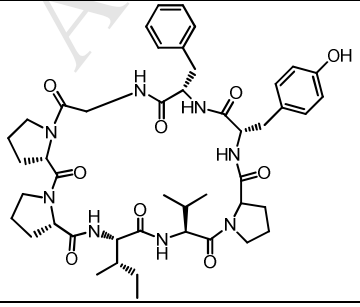	Solid phase & in solution chemistry

5e	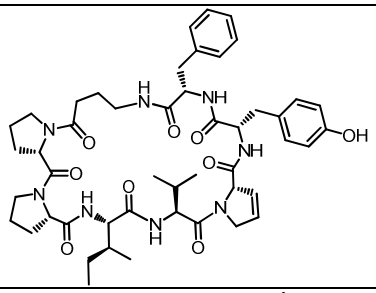	Solid phase & in solution chemistry
5f	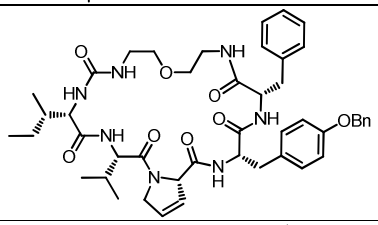	In solution chemistry
5g	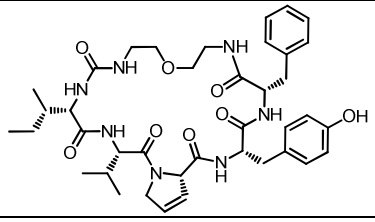	In solution chemistry
6a	$NH_2(CH_2)_3CO$-P-P-I-V-P-Y-F-COOH	Solid phase
6b	$NH_2(CH_2)_3CO$-P-P-I-V-G-Y-F-COOH	Solid phase
6c	$NH_2(CH_2)_2CO$-P-P-I-V-G-Y-F-COOH	Solid phase
6d	NH_2-G-P-P-I-V-G-Y-F-COOH	Solid phase
6e	$NH_2(CH_2)_3CO$-P-P-I-V-(DH)P-Y-F-COOH	Solid phase & in solution chemistry
6f	$NH_2(CH_2)_2O(CH_2)_2NHCO$-I-V-(DH)P-Y(Bn)-F-COOH	In solution chemistry

2. Results and discussion

2.1. Chemistry

The linear and the cyclic peptides object of this study were synthesized by combining solid phase and in solution synthesis. Table 1 summarizes all the linear and cyclic peptides herein described and the type of synthesis employed for their development. Compounds **2a,b**, **3a,b, 4**, and **6a-e** were synthesized by solid phase synthesis under microwave irradiation (Schemes 1-3) by applying a classical Fmoc chemistry while **6f** was synthesized as described in Scheme 4, entirely by in solution

chemistry. The cyclic peptides **5a-g** were obtained from their linear precursors by classical in solution chemistry using the appropriate condensing agent (Schemes 3 and 4).

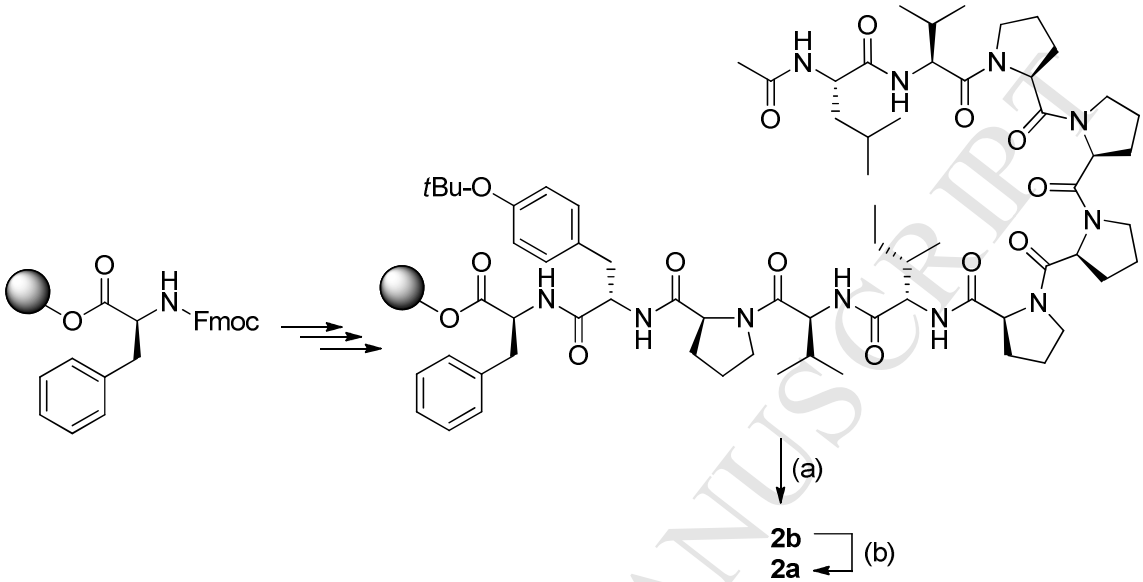

Scheme 1. Synthesis of the linear undecapeptides **2a** and **2b.** Reagents and conditions: (a) TFA/(*i*-Pr)$_3$SiH/H$_2$O 95:2.5:2.5, 25 °C, 3 h; (b) EEDQ, NH$_4$HCO$_3$, MeCN, 25 °C, 12 h.

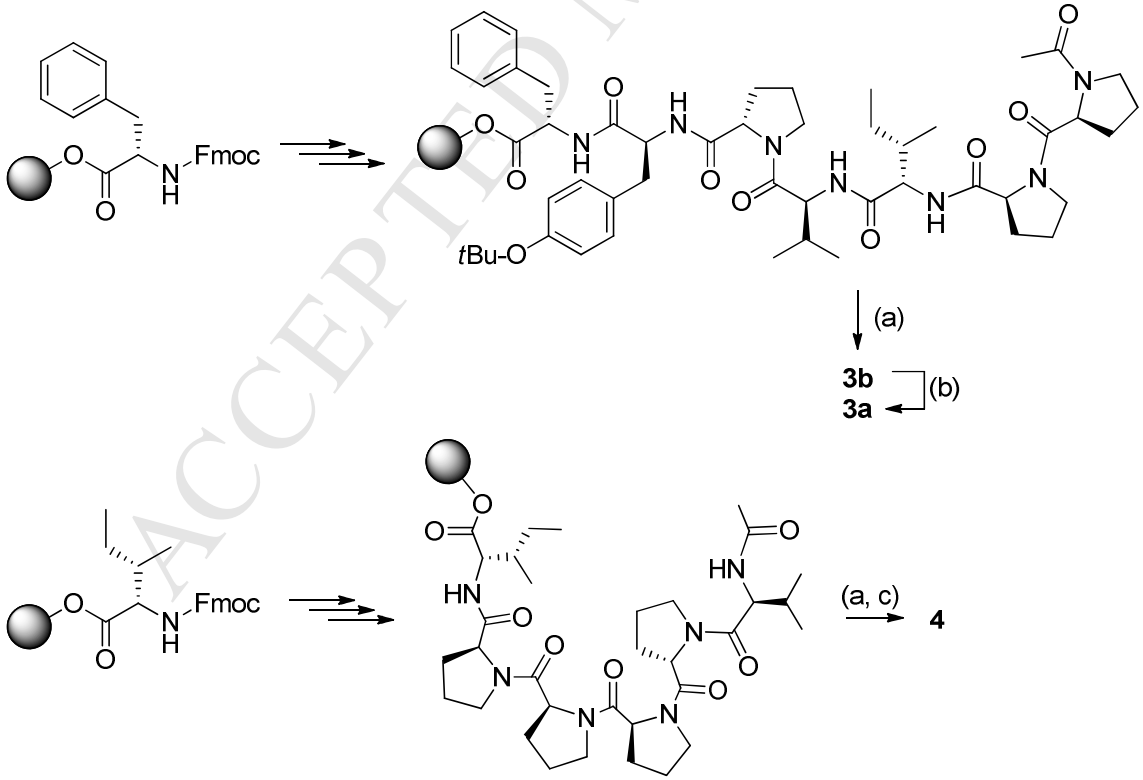

Scheme 2. Synthesis of the "disconnected" derivatives **3a,b** and **4.** Reagents and conditions: (a) TFA/(*i*-Pr)$_3$SiH/H$_2$O 95:2.5:2.5, 25 °C, 3 h; (b) EDCI, HOBt, DIPEA, NH(Me)$_2$·HCl, dry DCM, 0 °C to 25 °C, 12 h; (c) EEDQ, NH$_4$HCO$_3$, MeCN, 25 °C, 12 h.

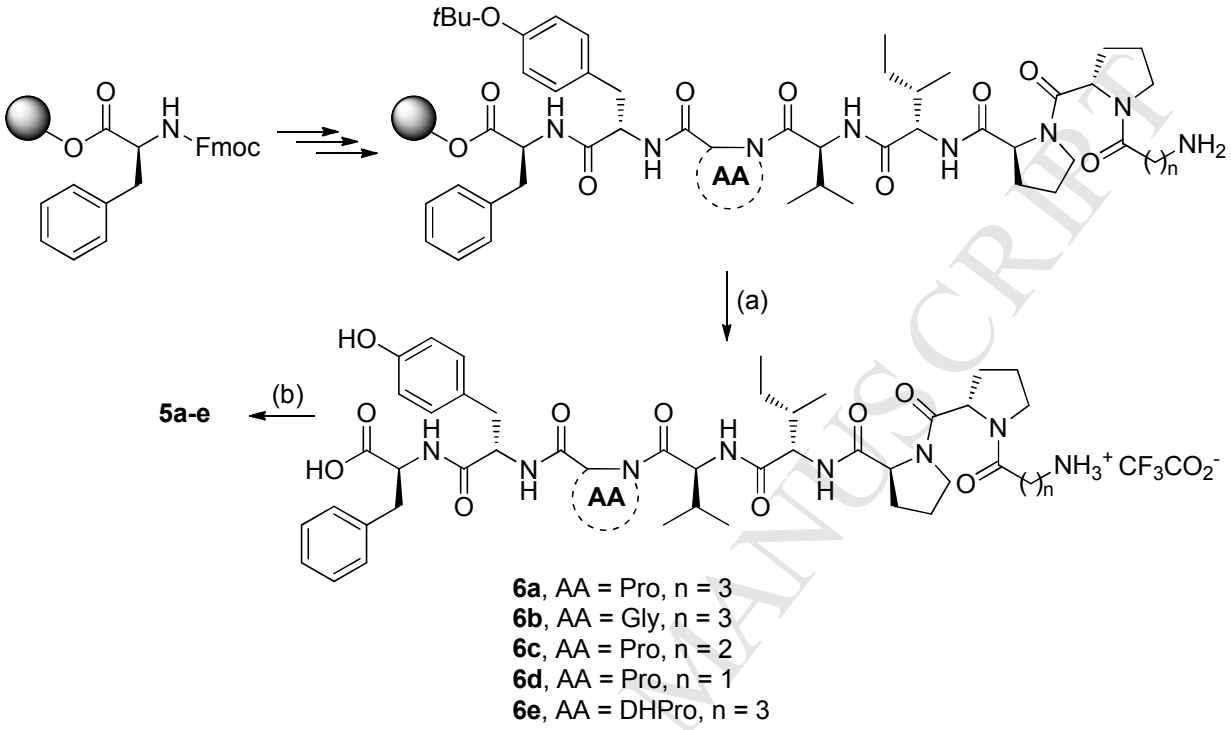

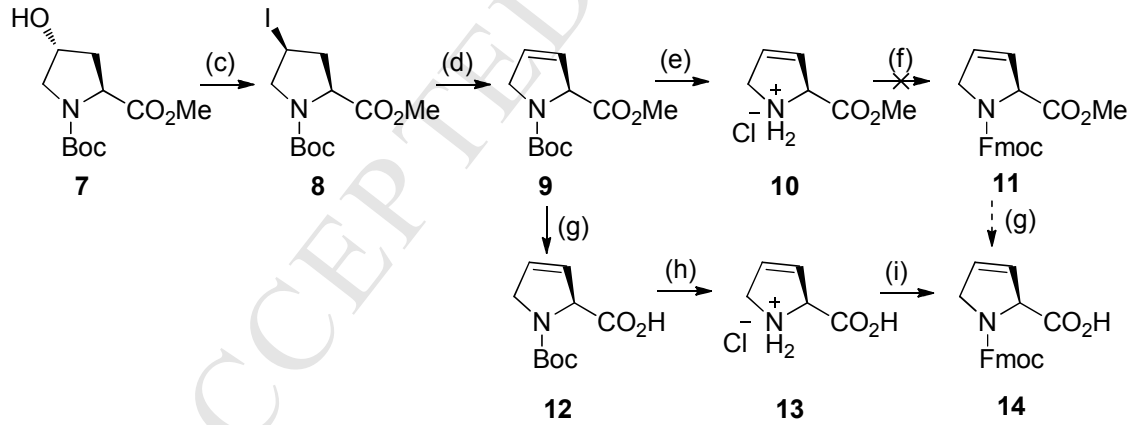

Scheme 3. Synthesis of the cyclic peptides **5a-e**, their linear precursors **6a-e**, and the dehydroproline **14.** Reagents and conditions: (a) TFA/(*i*-Pr)$_3$SiH/H$_2$O 95:2.5:2.5, 25 °C, 3 h; (b) HATU, HOBt, DIPEA, dry DCM, 25 °C, 12 h; (c) MeI, PPh$_3$, DIAD, dry THF, 0 °C to 25 °C, 12 h; (d) DBU, dry toluene, 85 °C, 3 h then 25 °C, 12 h; (e) AcCl, MeOH, 40 °C, 15 min; (f) Fmoc-Cl, TEA, dry DCM, 0 °C to 25 °C, 12 h; (g) LiOH, THF, MeOH, H$_2$O, 25 °C, 3 h; (h) TFA, dry DCM, 25 °C, 2 h; (i) Fmoc-Cl, Na$_2$CO$_3$, 1,4-dioxane, 25 °C, 12 h.

The synthesis of the linear peptides outlined in Schemes 1, 2, and 3 was performed following a solid phase approach, starting from a Wang resin functionalized with *N*-Fmoc-(*L*)-Phe, and using a standard Fmoc methodology in a CEM Liberty Automated Microwave Peptide Synthesizer. The peptides were released from the solid support by treatment with a mixture of TFA/(*i*-Pr)$_3$SiH/H$_2$O (95:2.5:2.5). The free carboxylic acid moiety of peptide **2b** was then converted into the corresponding primary amide (**2a**) by using EEDQ in presence of NH_4HCO_3 (Scheme 1). The same protocol was followed for the synthesis of peptide **4** while peptide **3a** was converted into the corresponding dimethylamide derivative **3b**, by classical coupling reaction with the hydrochloride salt of dimethylamine (Scheme 2). Scheme 3 describes the synthesis of **6a-e** and their cyclic counterpart **5a-e**. The peptides **6a-e**, obtained as described for **2b**, were dissolved in dry dichloromethane (DCM) at a concentration of 10^{-5} M and were cyclized by using HATU and HOBt as coupling agents. The *N*-Fmoc protected *S*-dehydroproline **14** needed for the synthesis of compound **6e** was prepared following the procedure reported in Scheme 3. Starting from the commercially available 4-hydroxy proline **7**, Mitsunobu reaction allowed its transformation into the corresponding iodinated derivative **8** which underwent an elimination reaction in the presence of DBU, to give the *N*-Boc protected *S*-dehydroproline **9**. After Boc removal (**10**, needed for the synthesis of **5f**) the *N* protection as 9-fluorenylmethyl carbamate was not successful and only afforded traces of the ester **11**. Thus, compound **14** was obtained by and alternative route where the hydrolysis of ester **9**, with an aqueous solution of LiOH (**12**), followed by Boc removal (**13**) and *N*-Fmoc protection led to the desired intermediate in good yield.

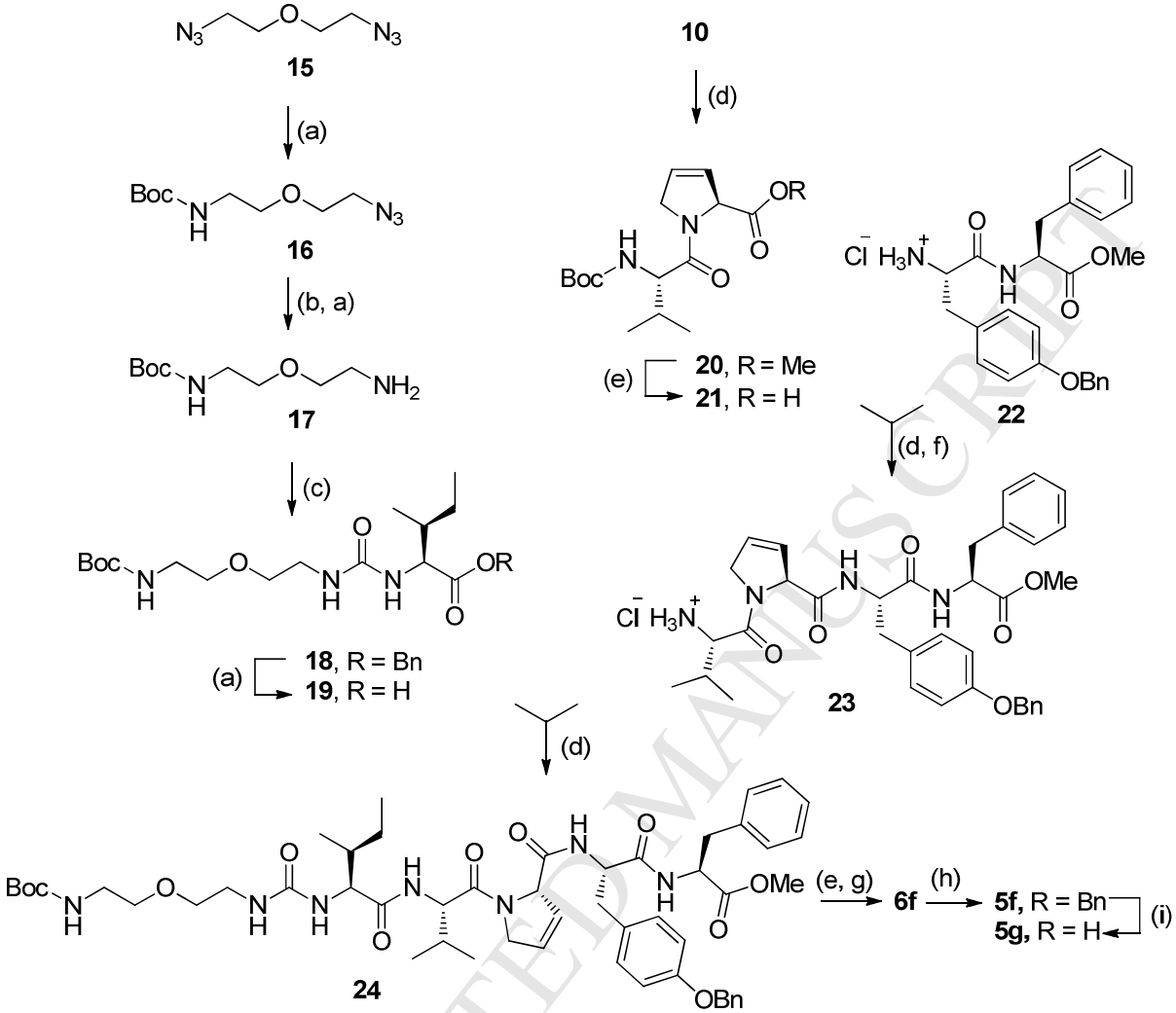

Scheme 4. Synthesis of the cyclic peptides **5f** and **5g.** Reagents and conditions: (a) H_2, Pd/C, MeOH, 2 h; (b) Di-*tert*-butyl dicarbonate, TEA, dry DCM, rt, 12 h; (c) (*L*)-Ile-OBn, $COCl_2$ 20% in toluene, $NaHCO_3$ ss, DCM, 0 °C to rt, 15 min then TEA, dry DCM, rt, 12 h; (d) *N*-Boc-(*L*)-Valine for **20**, EDCI, HOBt, DIEA, dry DCM, 0 °C to rt, 12 h; (e) LiOH, THF, MeOH, H_2O, rt, 3 h; (f) AcCl, MeOH, 40 °C, 15 min; (g) TFA, DCM, rt, 2 h; (h) HATU, HOBt, DIEA, dry DCM, 0 °C to rt, 12 h; (i) BCl_3, dry DCM, -78 °C to rt, 12 h.

The synthesis of compounds **5f** and **5g** was performed as outlined in Scheme 4. The diazidoethylether **15**, synthesized according to a reported procedure,[14] was subjected to a catalytic hydrogenation, followed by protection of the amine functionality with di-*tert*-butyl dicarbonate, and the obtained mono-protected intermediate **16** underwent a second reduction to afford the free amine **17**. This latter

was used as the nucleophile in the reaction with the isocyanate synthesized from H_2N-*L*-Ile-OBn with phosgene, for obtaining the intermediate urea **18** which was debenzylated by catalytic hydrogenation. The unnatural aminoacid *L*-dehydroproline **10**, obtained as reported in Scheme 3,[15] was employed in a classical in-solution coupling reaction with *N*-Boc-(*L*)-Val to afford dipeptide **20**, which was converted into the corresponding free acid (**21**) by hydrolysis with aqueous LiOH. In parallel the hydrochloride salt of the dipeptide **22** was obtained after coupling of the appropriately orthogonally protected amino acids (Boc-*L*-Tyr(OBn)-OH and NH_2-*L*-Phe-OMe) and deprotection of the amine functionality, by a methanolic solution of HCl. The dipeptides **21** and **22** were classically coupled, in the presence of EDCI and HOBt as condensing agents, and deprotection of the obtained compound afforded amine **23** to be used in the last coupling reaction with the previously synthesized intermediate **19**. The obtained linear compound **24**, after deprotection at both the C and N terminal ends (with aqueous LiOH, and with TFA respectively) yelded **6f** that was submitted to the cyclization reaction with HATU and HOBt as coupling agents. The obtained cyclic peptide **5f** was then treated with BCl_3 to afford the debenzylated compound **5g**.

*2.2. Conformational flexibility of linear peptide **2a** versus the cyclic peptide **5a**: NMR and computational studies*

In order to define the key structural features that could be relevant for the activity of our lead **2a**, we performed a detailed NMR structural analysis aiming at clarifying its structure in solution and we compared the data with the mimicked portion of Nur77. To perform NMR studies, we synthesized **2b** as a water soluble counterpart of **2a**. Preliminarily a primary 3D peptide structure of **2a** from sequence information was generated by submitting its amino acid sequence to *PEP-FOLD* [16, 17] and *PEPstr* [18] servers. The sequence analysis performed by means of *PEP-FOLD* resulted in six clusters of

structures all characterized by similar energies, thus indicating the convergence towards affordable conformations (Fig. S1 of the Supplementary Information (SI)).

As expected for an undecapeptide lacking secondary structure elements, we got divergent results by applying *PEPstr* analysis. *PEPstr* predicts a peptide secondary structure by applying the PSIPRED algorithm, [19, 20] and it generates a starting conformation with φ and ψ dihedral angle values corresponding to the previously predicted secondary structure. Using *AMBER 14*[21], energy minimization and molecular dynamics simulations of the initial conformation were performed. This analysis revealed a more "extended" conformation of **2a** compared to the corresponding Nur77 region. Our data revealed that **2a** conformation also embeds a type IV β-turn in the poly-prolyl region (Fig. S2).

This conformational analysis was essentially confirmed by NMR studies. As reported in the Experimental Section **2b** spectra were acquired in D_2O and H_2O/D_2O as solvent. All the proton resonances were assigned using a combination of correlation spectroscopy (COSY), total correlation spectroscopy (TOCSY) and nuclear Overhauser enhancement spectroscopy (NOESY) experiments. Residue-specific assignment was achieved from TOCSY spectra, by recognizing the unique spin system for each residue. For most of the residues, starting from the amidic proton, it was possible to reconstruct the connectivity pathway, by comparing the TOCSY and the COSY spectra (Fig. S3). Complete assignment is given in Table S1.

The main feature of NMR conformational analysis is the accurate estimation of structural restraints. In fact, NOE intensities and coupling constants (*J*) account for distance and torsional restraints respectively.

Overall our NMR analysis revealed for **2b** a random coil structure, indicating the need of analogues with reduced conformational flexibility to address the binding mode. Consequently, the cyclic conformationally constrained peptides typified by **5a** were synthesized.

A total of 82 and 99 peak volumes were integrated from the NOESY spectra of **2b** and **5a** respectively. In the spectrum of **2b** a region with opposite-phased peaks (compared to all the other peaks) was observed (Fig. S4). The related resonances belong to the Phe11 residue; this accounted for a distinct flexibility of this residue with respect to the overall tumbling rate of the peptide.

The $^{3}J_{NH\alpha}$ for both **2b** and **5a** were directly measured from the splitting observed on the amide proton resonances. All the NH groups of **2b** showed similar coupling constants in the range of 6÷7 Hz (Table 2), indicating a random coil structure. In fact, small linear peptides usually present averaged $^{3}J_{NH\alpha}$ values of 7.4 Hz, indicating that the peptide lacks a single stable conformation. On the contrary, with **5a** the observed $^{3}J_{NH\alpha}$ values (Table 2) strongly suggested that the molecule adopts a preferred conformation.

Table 2. Measured $^{3}J_{NH\alpha}$ for **2b** and **5a** amide hydrogen atoms. All the values are characteristic of random coil dihedral angles, suggesting the absence of a single favored conformation.

2b Residue	$^{3}J_{NH\alpha}$	**5a Residue**	$^{3}J_{NH\alpha}$
Leu1	6.58	Spacer 1-a	1.53
Val2	7.67	Spacer 1-b	9.43
Ile7	7.45	Ile3	5.70
Val8	7.67	Val3	overlapped
Tyr10	7.23	Tyr6	6.58
Phe11	7.89	Phe7	9.57

To further confirm the low structural flexibility of **5a** compared to **2a,b**, we performed temperature dependence experiments. This analysis demonstrated that the $^{3}J_{NH\alpha}$ coupling constants were not affected by temperature variation, thus indicating that **5a** adopts a particularly stable conformation.

Notably, at 323 K and 328 K, the spacer amide peak of **5a** did not overlap to aromatic resonances, an event that allowed us to identify the two well-defined $^{3}J_{NH\gamma}$ constants (between the NH and the two diasterotopic γ methylenes hydrogen atoms of the spacer).

H-bond is one of the major interactions contributing to the stabilization of secondary structures in proteins, and delineation of H-bonds is relevant for assessing peptide conformations. Accordingly, H-bond network involving amide protons has been defined by temperature dependence experiments. From NH chemical shift analysis, we could identify the exposed or shielded (H-bonded) NH in our peptide sequences. In fact, amide shielded protons show a lower temperature dependence of their chemical shifts (usually defined as δ(ppm)/*T(K)* ratio or Temperature coefficient, *Tc*) compared to exposed protons.[22] A |*Tc*| < 3 ppb/K is indicative of intra-molecular H-bond formation of the shielded protons, whereas a |*Tc*| > 5 ppb/K likely represents exposed amide protons.[22, 23]

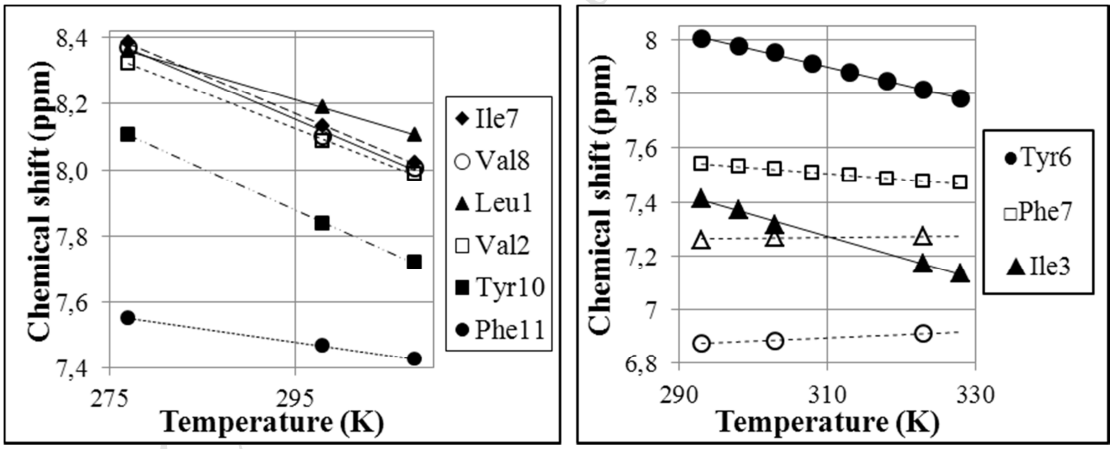

Fig. 3. Temperature dependence of the chemical shifts of the amide protons of **2b** (left) and **5a** (right).

The quantitative plot of the analysis of these data (Fig. 3) further underlines the different behavior of **2b** and **5a** amide H atoms.

The *Tc* were calculated for each residue and defined as the slope of the best-fit line (Table S2). Concerning **5a**, amide NH protons of the spacer, Val5 and Phe8 residues, are likely intra-molecular H-

bonded in the majority of conformers. On the contrary, *Tc* values from **2b** amides were all characteristic of solvent exposed hydrogen (|*Tc*| > 5ppb/K), with the only exception of Phe11 NH (|*Tc*| = 4 ppb/K). In the latter case, this intermediate *Tc* value did not unambiguously indicate the presence of a H-bond. For random coil peptides in aqueous medium (as **2b**) the *Tc* parameter is often unreliable.[22, 24] However, since Phe11 amide peak of **2b** was also the only NH peak which did not undergo line broadening at high temperatures, the hypothesis of a H-bond involving this residue could not be completely ruled out; alternatively we can hypothesize a solvent protection of Phe11 amide for a minor population of conformers of **2b**. Moreover, the narrow resonances recorded on the NMR spectra, at variable concentrations, suggest that the linear peptide did not undergo aggregation.

2.3. Molecular Modelling Studies.

In order to understand the potential ability of our lead cyclic peptide (**5a**) to mimic the region of Nur77 which can bind Bcl-2 and β-tubulin[13] (see Fig. 4A), we initially performed an extensive conformational search analysis by means of MacroModel,[25] to evaluate the possibility of lower energy conformers of **5a** to form an intramolecular H-bond as highlighted by NMR studies and which reproduces the same H-bond as evidenced in Nur77 X-ray structure (PDB ID 1YJE) (Fig. 4A,B).

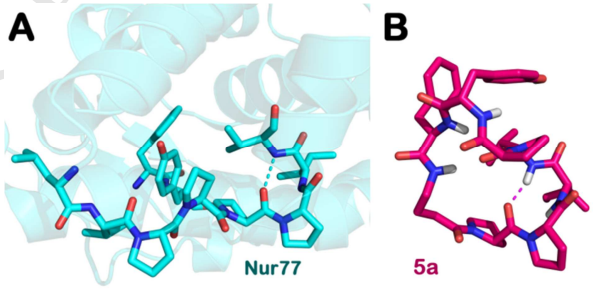

Fig. 4. (A) Crystal structure of Nur77 (PDB ID 1YJE) highlighting the β-tubulin and Bcl-2 interacting portion represented as cyan sticks; (B) Low energy conformer (-542.454 kcal/mol) of **5a** represented by magenta sticks. Intramolecular H-bonds are represented by dotted lines. The pictures were generated by means of PyMOL.[26]

Our studies highlighted a high degree of 3D arrangement similarity between the lower energy conformer of **5a** (Fig. 4B) and the Nur77 binding region. In fact, the region of Nur77 where the H-bond is detected (PDB ID 1YJE) (between V587 and P584 mouse numbering) is superimposable to the corresponding area of the low energy conformer of **5a** where the intramolecular H-bond between Pro7 and Val4 was proved by NMR analysis. This feature allows **5a** to reproduce the relevant motif of Nur77 for binding its targets.[13]

Since we already demonstrated that **1** mimics the Nur77 binding region,[13] we hypothesized that the cyclic peptide **5a** might share (although partially) with **1** the same binding site on β-tubulin. To confirm this hypothesis we have performed a blind docking calculation considering both α- and β-tubulin subunits by using Autodock.[27-32] Autodock software is able to accomplish the blind docking of compounds and to select the correct complexes based on energy without prior knowledge of the binding site. The output of this approach (Fig. 5) clearly shows that the preferred binding site for the lower energy poses of **5a** overlaps to that of **1**. On the β-tubulin subunit, no poses were found in the colchicine binding site, while a very limited number of solutions was found matching with the vinblastine binding site, the analysis of which revealed much less favourable docking scores when compared to those found for **5a** into the PTX-binding site. Accordingly, the vinblastine binding site appeared not suitable for **5a**/β-tubulin interaction. Notably, a very limited number of docked solutions were found on α-tubulin. These poses did not cover the binding site of known drugs (pironetin, and griseofulvin) and, being devoid of relevant docking scores, allowed us to exclude the α-tubulin subunit as a putative target for **5a**. Overall, these findings indicate the PTX-binding site on β-tubulin as the most reliable binding site for **5a**.

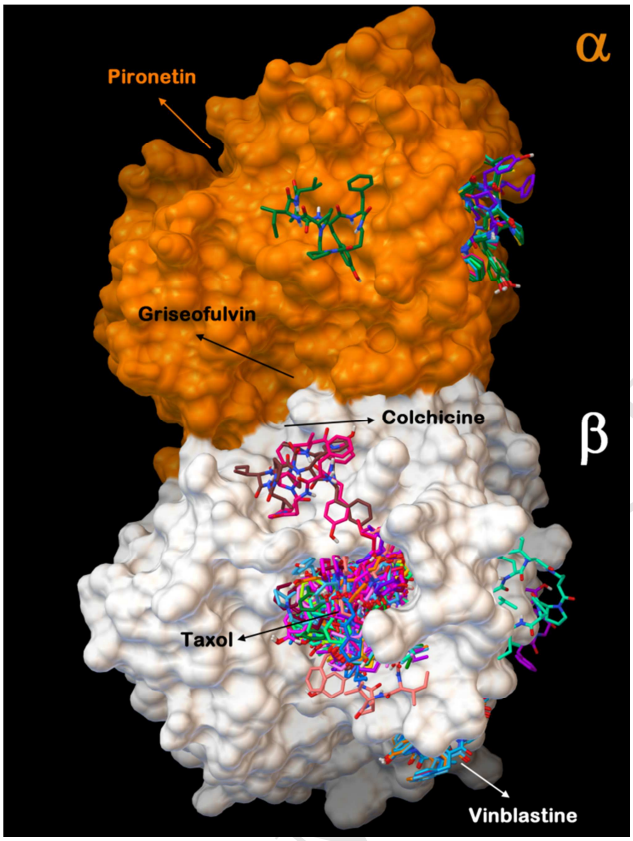

Fig. 5. Blind docking output for **5a** (coloured sticks) against α/β-tubulin (orange and white surfaces, respectively). In the picture the known tubulin binding sites have been reported. The picture was generated by Autodock.[32]

Additional computational studies were performed for investigating the influence of the cycle size on the binding mode of a set of cyclic peptides when gradually shortening the butyric chain of **5a** (as in compounds **5c**, and **5d**, Fig.1 and Table 1). The potential binding modes of compounds **5a**, **5c**, and **5d** on β-tubulin were then analysed by means of GOLD software that employs genetic algorithm[33-35] on the binding site of **1**. These studies were coupled to the estimation of free binding energy (Prime MM/GBSA[36] implemented in Maestro suite[37]) as previously reported by us[38-42] also for evaluating the binding modes of peptide-like compounds.[43, 44] The output of this calculation is reported in Fig. 6A-D for **5a**, **5c**, **5d**, and **5f**. Analysis of the data revealed that **5a** interacts within its

putative binding site through a series of polar and hydrophobic contacts. In particular, we observed a series of H-bonds with R278 and T276, while a cation-π stacking could be established between the Tyr residue of **5a** and R369 while the closer Pro was easily accommodated into a hydrophobic sub-pocket formed by residues F272, P360 and L371. The Phe residue of **5a** was involved in a π-π stacking with H229. These major contacts might support a good fitting of **5a** in the PTX-binding site. Notably, as a further validation of this data, the same pose was found as the top-ranked pose during the blind docking calculation. The superposition of the pose of **5a** from the blind docking (Autodock) and the docking calculation (GOLD) is provided in Fig. S5. The used protocol was able to reproduce the crystallized pose of **1** (PDB ID 1JFF) further supporting our computational approach.

For compound **5c**, the obtained docking output (Fig. 6B) was slightly different from that found for **5a**. Particularly, **5c** was found to be more deeply accommodated into the binding pocket. This may be due to a strong H-bond network found between R369 and the Tyr residue of **5c** which in turn allowed an increase of contacts especially in terms of hydrophobic interactions. In fact, in addition to the H-bonds and the hydrophobic contacts above mentioned for **5a**, **5c** was also able to establish a π-π stacking with F272 by its Tyr residue. Moreover the Pro closer to the Tyr residue is involved in a series of hydrophobic contacts with P360 and V23. The two other Pro residues were found to form hydrophobic contacts with P274, L286, and L371.

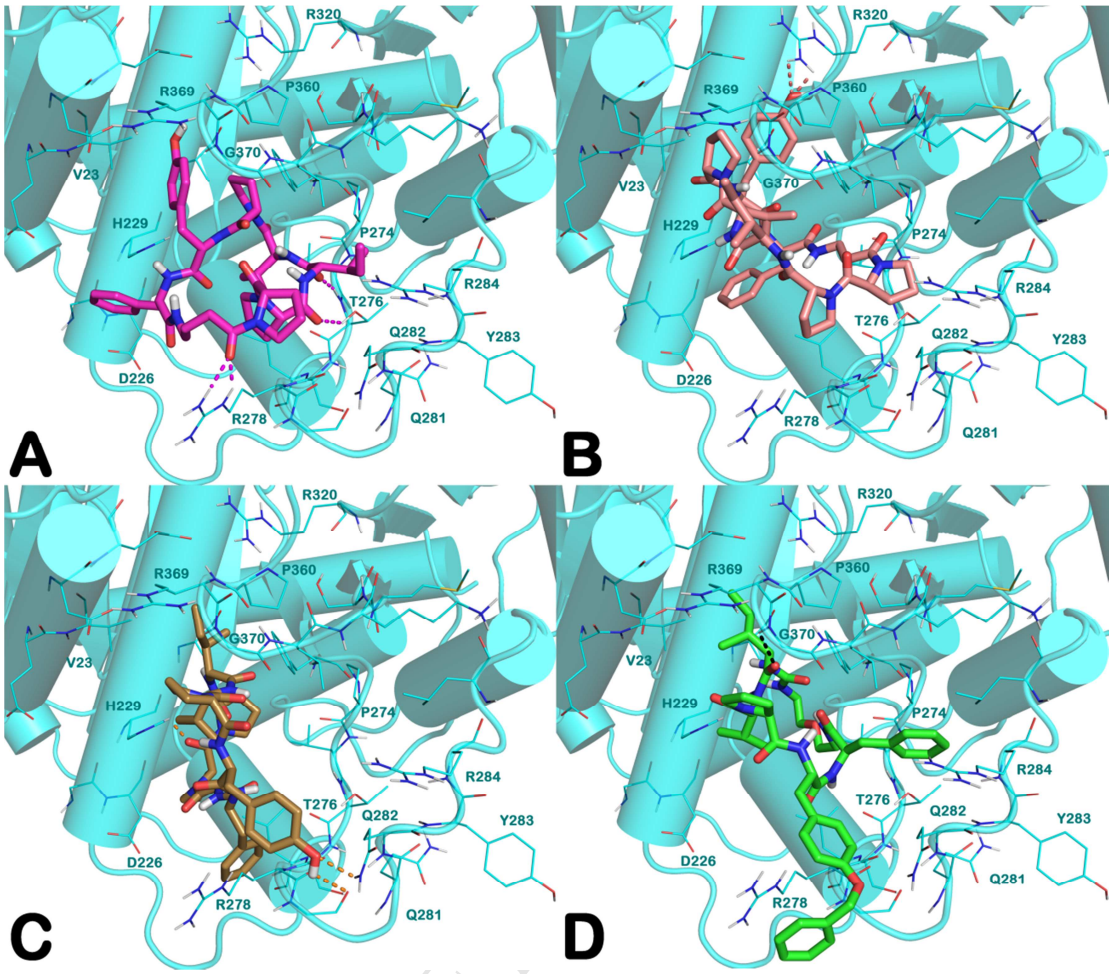

Fig. 6. (A) **5a** (magenta sticks) (B) **5c** (light pink sticks) (C) **5d** (gold sticks) and (D) **5f** (green sticks) into the β-tubulin PTX-binding site (cyan cartoon). The residues located in the binding site are represented by lines. H-bonds are represented by dotted lines. Nonpolar hydrogens were omitted for the sake of clarity. The pictures were generated by PyMOL.

A progressive restriction of the ring dimension led to compound **5d** (Fig. 6C) for which our computational studies revealed a different orientation of the docked poses belonging to the most populated cluster. In fact the aromatic moieties of **5d** were accommodated at the boundary of the binding site, strongly interacting by H-bonds with R278, G279, and Q281 by its Tyr portion. The Phe portion established a cation-π stacking with R278. Moreover H-bond with H229 and hydrophobic interactions of Ile moiety (**5d**) stabilized the docked pose. In fact, Ile moiety is involved in a series of

hydrophobic contacts with P360, F272, and V23, while the Pro residues closer to Phe portion established hydrophobic contacts with L217, L219 and L275. Compounds **5f** and **5g** were conceived to further reduce the peptide character of our cyclic compounds. Two further proline residues and the spacer of **5a** were replaced by an ethereal chain linked by an ureidic bond to the Ile5, while maintaining the DHPro into the structure. Notably, as shown in Fig. 6D, **5f** spans the entire binding site on tubulin, interacting with the backbone of G370 by H-bond, while its benzylated Tyr residue enables a double cation-π stacking with R278. Furthermore, the central region of **5f** produced a series of hydrophobic interactions principally by its Phe moiety which is deeply located in a hydrophobic sub-pocket formed by P274, A285 and L286. Moreover, the Phe lateral chain of **5f** may form another cation-π stacking with R284. In compound **5g** the lack of the benzyl group did not allow to establish a binding mode as that found for **5f**. In fact, the interactions around R278 were completely lost by **5g** and these contacts were not replaced by other interactions. These features did not allow **5g** to occupy the entire binding cleft thus resulting in a relevant solvent exposed portion of the compound and in a large number of clustered docking solutions. This event produced an inconsistent binding mode which is nonetheless in agreement with the poor pro-apoptotic potential of the compound (see Table S4). In general all the computational studies are in agreement with the cellular data reported in Table S4 Table 3 and Figures 7 and 8.

2.4. Cellular studies

*2.4.1. Cyclic peptides **5a-d,f** promote apoptosis in cancer cell lines*

Preliminary flow cytometric sub-G_0/G_1 analysis EBV-B (Epstein-Barr Virus (EBV)-immortalized B cells), Jurkat (human T lymphocyte), and HL60 (human promyelocytic leukemia) cell lines treated under identical conditions with either **5a** and **2a** (25 μM) evidenced that the cyclic peptide but not the linear peptide was able to induce apoptosis after 24 h of incubation (Table S3). Following this initial

screening, and in order to understand if the novel compounds might promote apoptosis, intranucleosomal DNA fragmentation, a major hallmark of apoptotic cell death, was determined by flow cytometry [45] on HL60 cells treated with both cyclic (**5a-g**) or linear (**2a,b** and **6a-f**) peptides (Fig. 7 and Table S4). The results show that cyclic peptides **5a,c,d,f**, but not **5b**, **5e** and **5g** or linear peptides, induced a significant enhancement in the percentage of apoptotic cells (with hypodiploid or ''sub-G_0/G_1'' DNA content) compared with vehicle (Fig. 7A). In fact, compound **5e**, which incorporates the unnatural amino acid 3,4-dehydro-(*L*)-proline (DHPro) into its structure in place of Pro3 of **5a**, almost completely lost its pro-apoptotic potential (Table S4). Moreover, in agreement with our computational studies, **5f** improved the pro-apoptotic effect of our lead **5a** while no appreciable activity was observed with **5g** (Table S4).

Interestingly, differently from **1**, treatment with compounds **5a**, **5c**, **5d** and **5f** resulted in a higher and dose dependent percentage of cells in sub-G_0/G_1 phase which was paralleled by a significant reduction in the percentage of cells in G_0/G_1 and G_2/M phases confirming that these novel compounds induce cell death by apoptosis (Fig. 7A). The efficacy of these compounds, when tested at 50 μM for 24 h, ranged from 33.1% induction of apoptotic cells for compound **5c** to the 77% for compound **5f** (Table S4 and Fig. 7A) when compared to untreated cells.

Interestingly our prototypical compound **5a**, which behaved as one of the best performing cyclic peptides, was found to induce apoptosis in various tumor cell lines (Table 3) thus indicating a broad-spectrum activity.

Consistent with the pro-apoptotic effect of **5a**, **5c**, **5d**, and **5f** on HL60 cells, externalization of phosphatidylserine, which normally resides in the inner plasma membrane of healthy cells, was significantly enhanced as compared to cells treated with vehicle, as assessed by flow cytometric analysis of Annexin-V (Fig. 7A).

Mitochondria are at the crossroads of the two main apoptotic signaling pathway, namely the intrinsic and extrinsic pathways, and their integrity is moreover tightly controlled by the Bcl-2 family of proteins.[46-48] To understand if **5a**, **5c**, **5d** and **5f** induce apoptosis by targeting mitochondria we measured the dissipation of mitochondrial inner transmembrane potential ($\Delta\Psi$ m) by flow cytometry in tetramethylrhodamine methyl ester perchlorate (TMRM) loaded cells. A significant increase in the percentage of cells with loss of mitochondrial inner transmembrane potential was found following treatment with cyclic peptides **5a**, **5c**, **5d** and **5f** compared with vehicle (Fig. 7B) indicating that these novel compounds induced apoptosis by targeting the mitochondria.

Collectively, the results provide evidence that cyclic peptides **5a**, **5c**, **5d** and **5f** are able to induce cell death by apoptosis through a mitochondrial dependent pathway with **5a** and **5f** being the most active of the series.

To further asses the efficacy profile of this newly identified class of pro-apoptotic agents our prototypical compound **5a**, and some analogues, were also tested on small set of solid tumor cell lines (Fig. 8). Flow cytometry analysis of the MCF-7 breast cancer cell lines treated with **5a** (50 µM) for 24 h, showed a modest pro-apoptotic effect (11.8% apoptosis compared to 8.5% in vehicle-treated cells). This was slightly lower than the level of apoptosis observed when the same cell line was treated with compounds **5c** and **5d** (18.9% and 17.3% apoptosis, respectively). Compound **2a** was inactive when tested on the MCF-7 cell line.

The effect of **5a** and **2a** was also evaluated in murine and human melanoma cell lines. Flow cytometric analysis of both B16F1 (less metastatic) and B16F10 (more metastatic) mouse melanoma cells incubated with **5a** (50 µM) for 24 h revealed a small percentage of apoptotic cells (as sub-G_0/G_1 %) when compared to the respective controls (Table 3). Furthermore, flow cytometric analysis of two human melanoma cell lines (the less metastatic A375 and more metastatic 501Mel cell line) treated

with **2a** and **5a**, showed that **2a** was inactive in both cell lines, when tested at 100 μM, while **5a** displayed significant pro-apoptotic effects in the less metastatic A237 cell line eliciting 48% apoptosis when tested at 50 μM with an incubation time of 72 h (Table 3).

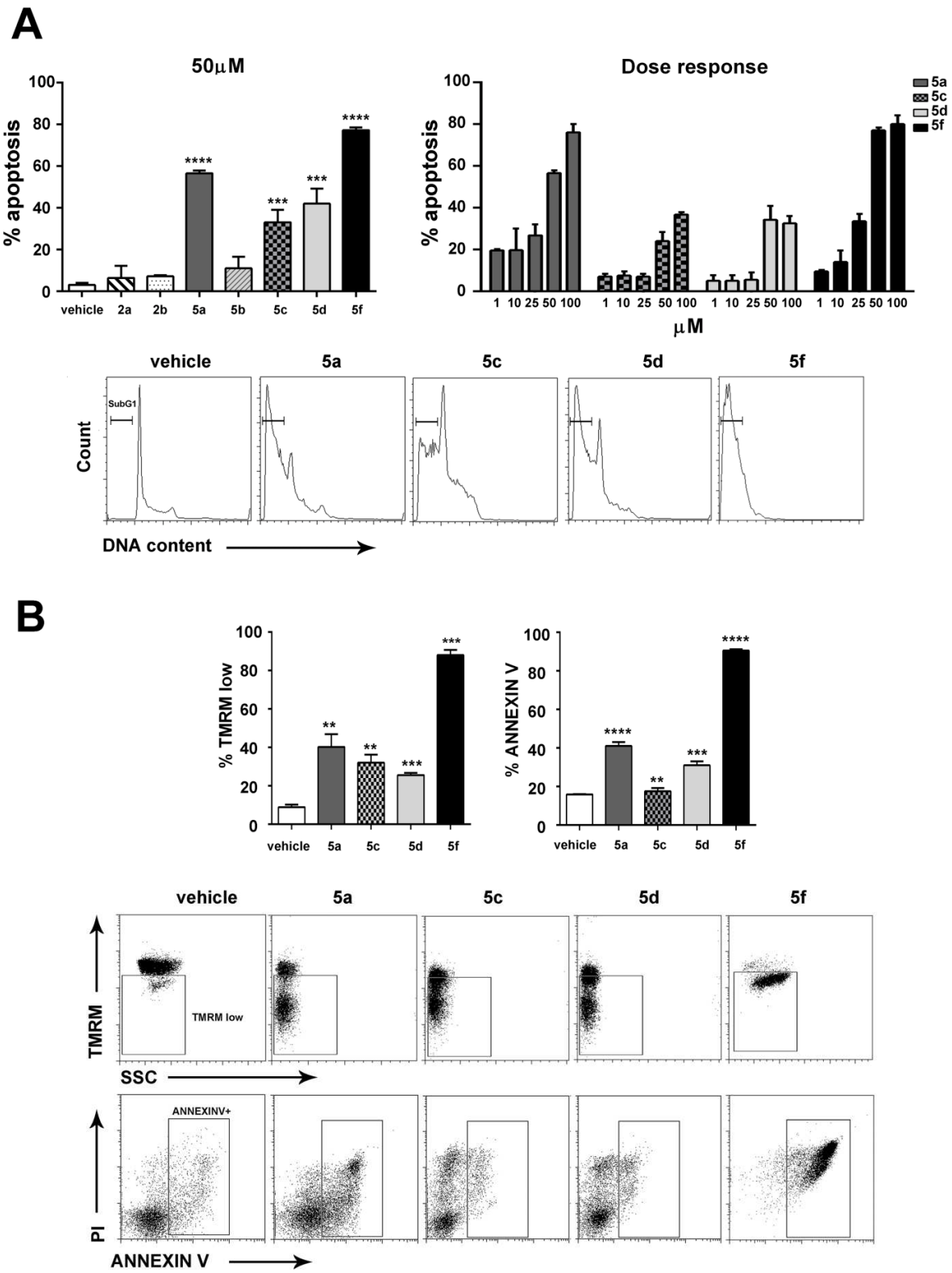

Fig. 7. Cyclic peptidomimetics induce apoptosis in HL60 cells. (A) Cells were treated with 50 μM **2a,b**, **5a-d,f** for 24 h and DNA content was measured by flow cytometry. Control samples were treated with vehicle (0.1% DMSO). Alternatively cells were treated with 1, 10, 25, 50 and 100 μM **5a-d,f**. The

bar graphs show the percentage of cells in the sub-G_0/G_1 phase. Data are mean ± SD (n > 3), ****p< 0.0001 **5a** vs vehicle, ***p= 0.0002 **5c** vs vehicle, ***p= 0.0001 **5d** vs vehicle, ****p< 0.0001 **5f** vs vehicle. Representative histograms are shown. (B) Quantitation by flow cytometry of mitochondrial integrity in TMRM-loaded cells treated with 50 μM **5a-d,f** or with vehicle (0.1% DMSO) for 24 h. The bar graphs show the percentage of cells with depolarized mitochondria (TMRM low) cells. Data are mean ± SD (n > 3). **p = 0.0073 **5a** vs vehicle, *p = 0.016 **5c** vs vehicle, ***p = 0.0004 **5d** vs vehicle, ***p = 0.0008 **5f** vs vehicle. Quantitation by flow cytometry of Annexin V/PI staining of cells treated with 50 μM **5a-d,f** or with vehicle (0.1% DMSO) for 24 h. The bar graphs show the percentage of Annexin V^+ cells. Data are mean ± SD (n > 3). ****p < 0.0001 **5a** vs vehicle, **p = 0.011 **5c** vs vehicle, ***p = 0.0002 **5d** vs vehicle, ****p < 0.0001 **5f** vs vehicle. Representative dot plots are shown.

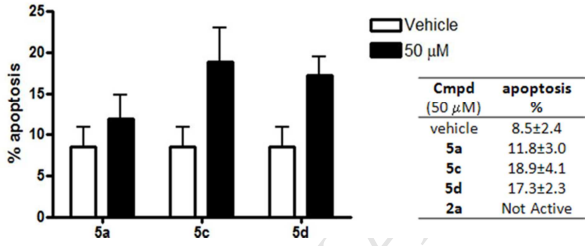

Cmpd (50 μM)	apoptosis %
vehicle	8.5±2.4
5a	11.8±3.0
5c	18.9±4.1
5d	17.3±2.3
2a	Not Active

Fig. 8. Effect of cyclic peptides **5a,c,d** on apoptosis in breast carcinoma cells. MCF-7 cells were treated with vehicle (0.1% DMSO) or 50 μM **5a**, **5c**, or **5d** for 48 h. The linear peptide **2a** was found inactive when tested under the same experimental conditions. Their DNA content was then analysed as described in the Experimental Section. Cells with less than 2N DNA content were deemed apoptotic. Values represent the mean ± SEM for three independent experiments.

Table 3. Efficacy of compounds **2a** and **5a** (at 50 μM concentration) on different melanoma cell lines as % of apoptosis (sub-G_0/G_1).

		Apoptosis %	
Cmpd→	**Vehicle**	**2a**	**5a**
Cell line↓			
B16F1	1.9±1.6	NA[b]	13.9±5.4
B16F10	3.7±3	NA[b]	13.6±1.8
A375	7±1	NA[b]	48±0.5[c]
501Mel	9±1.8	NA[b]	17±1.7[c]

[a]vehicle (0.1% DMSO); [b]NA: not active; [c]tested at 50 μM with 72 h of incubation time. All the values are the mean of at least three independent experiments.

*2.4.2. Both the cyclic peptide **5a** and the linear peptide **2a** enter into the cells and do not undergo metabolic inactivation.*

The differing efficacy of the cyclic *versus* the linear peptides was further investigated, by means of confocal microscopy and mass analysis of cell lysates, in order to understand whether the observed difference in cellular efficacy might be dependent upon cell permeability and/or on different metabolic stability of the (internalized) compounds.

Confocal microscopy analysis capitalized on the fact that these novel compounds behaved as fluorescent probes (with two emission maxima around 340 and 500 nm, not shown) thus allowing us to follow their cell permeability in confocal microscopy studies on HL60 cells without any derivatization. These experiments clearly showed that the cyclic peptide **5a** and the linear analogues **2a** and **2b** were all cell permeable (Fig. 9). We hypothesized that the lack of cellular effects of the linear peptides could be due to metabolic susceptibility. In fact, the use of peptides in the cellular environment is plagued by unwanted and rapid proteolysis exerted by exo- and endo-peptidases.[49] These enzymes are an integral part of the protein recycling machinery of cells and ensure that most peptides are rapidly hydrolyzed to their amino acid constituents. To address this issue we incubated **5a** and **2b** in HL60 cells at different concentrations and incubation times (6 h, 24 h and 48 h). Mass spectra analysis of the cellular lysates evidenced that both compounds were present inside the cells (Fig. S6), thus confirming cell permeability of these analogues, and also showed that both compounds were found within the cells up to 48 h of incubation. Although not quantitative, this methodology allow us to exclude that inefficacy of the linear undecapeptide **2a** could be ascribable to its more rapid metabolism as compared to **5a**.

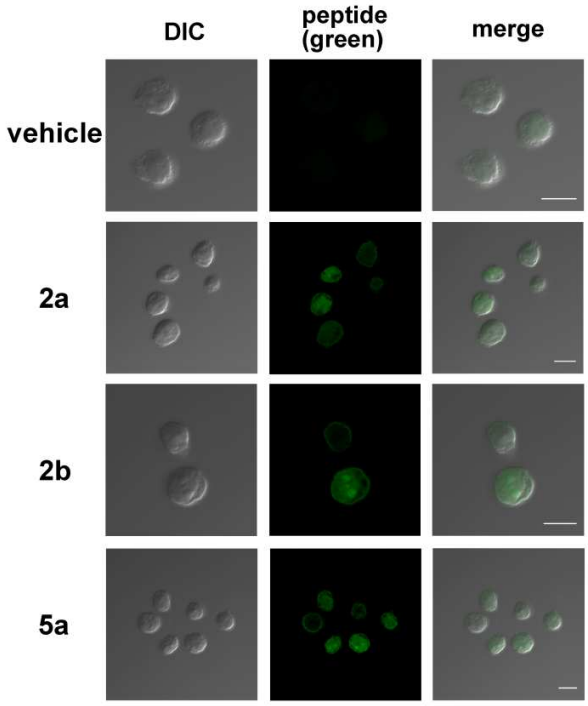

Fig. 9. Confocal microscopy analysis of HL60 cells incubated with linear peptides **2a,b** and the cyclic peptide **5a.** Scale bar, 10 μm.

2.4.3. Cyclic peptides affect microtubule dynamics

The effects of a representative analogue on the assembly of tubulin (porcine tubulin from Cytoskeleton) were evaluated. Compound **5c**, which demonstrated encouraging pro-apoptotic effects, was analyzed in an in vitro tubulin assay.

The turbidity assay is a convenient method for assessing the effects of drugs on tubulin polymerization or depolymerization, and is based on a spectrophotometric measurement of the light which is reflected by microtubules. When α/β-tubulin dimers polymerize into microtubules an increase in turbidity is detected. The equilibrium between α/β-tubulin dimers and microtubules is favored at 37 °C (physiological temperature) and depolymerization is induced at 2 °C. All microtubule stabilizer compounds accelerate this phenomenon, while the destabilizers induce depolymerization below the levels of the vehicle.

In our tests, the ability of **1** to effectively induce tubulin assembly was used as a positive control, while ethanol (1% v/v) was used as a vehicle control. Tubulin polymerization was determined by measuring the increase in absorbance over time at 340 nm. Since the V_{max} value is a sensitive indicator of tubulin/ligand interactions, the V_{max} values were calculated for the tested compound. Induction of tubulin polymerization for **5c** is illustrated in Fig. S7. We observed that a 100 μM concentration of the tested compound was able to induce a tubulin polymerization level comparable to that induced by **1** (10 μM) although over longer incubation times. These data indicate that this compound behaves as a tubulin stabilizer (100 μM) and is in line with the pro-apoptotic efficacy detected at 50 and 100 μM.

To further test the capability of the cyclic peptides of interfering with tubulin polymerization, we performed β-tubulin staining studies on the rat basophilic leukemia (RBL) cell line (RBL-2H3) which are relatively large cells such that their microtubules can be easily visualized. The cells, treated with the cyclic peptides **5a** and **5d** in comparison with vehicle and **1**, were stained with anti-β-tubulin monoclonal antibody followed by FITC-conjugated anti-mouse IgG. The results (Fig. 10) showed that **5a** and **5d** altered the microtubule network.

Collectively, these data allowed us to conclude that the pro-apoptotic effect of **5a** and **5d** may result from an alteration of microtubule dynamics.

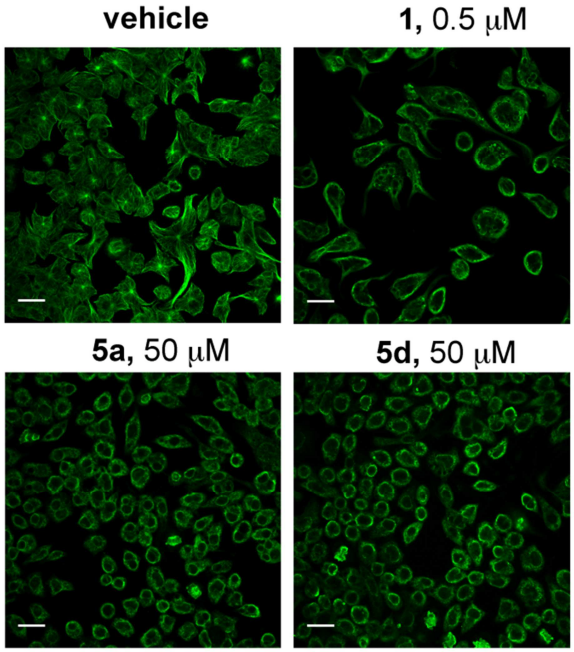

Fig. 10. Effects of **5a** and **5d** on microtubules. Representative confocal micrographs of the distribution of microtubules taken at equatorial planes of RBL-2H3 cells treated with the tested compounds (**5a** or **5d**, 50 μM), vehicle (0.1% DMSO) or **1** (0.5 μM) for 24 h and stained with anti-β-tubulin antibody. Scale bars, 20 μm (n = 3).

3. Conclusions

We have herein reported the development of pro-apoptotic cyclic peptides **5a-g**, linear peptides, **2b**, **3**, **4a,b** and **6a-f**, the synthesis of which was inspired by the undecapeptide **2a** which was developed as a mimetic of Nur77 and **1**. We have demonstrated that cyclic peptides, but not the linear peptides, are characterized by a pro-apoptotic effect on different cancer cell lines. The lack of cellular activity of the linear peptides may be suggestive of their difficulty to reach the correct spatial arrangement for eliciting a pro-apoptotic effect. This interpretation was supported by NMR studies on both **2b** and **5a**, and by computational studies. Additional studies demonstrating cell permeability (confocal microcopy)

and excluding metabolic inactivation of the linear peptide **2a** when compared to our cyclic lead **5a** (mass analysis of cell lysates) were also in agreement with our proposed hypothesis. Moreover, as a further advancement we have developed analogues of **5a** with a substantially lowered peptide character such as the potent pro-apoptotic cyclic compound **5f** which will pave the way to the design of further optimized pro-apoptotic agents.

4. Experimental Procedures

4.1. Chemistry

Starting materials and solvents were purchased from commercial suppliers and used without further purification. Reaction progress was monitored by TLC using silica gel 60 F254 (0.040-0.063 μm) with detection by UV. Silica gel 60 (0.040-0.063 μm) was used for column chromatography. Yields refer to purified materials and are not optimized. ^{1}H NMR and ^{13}C NMR spectra were recorded on a Varian 300 MHz or a Bruker 400 MHz spectrometer using the residual signal of the deuterated solvent as internal standard. Splitting patterns are described as singlet (s), doublet (d), triplet (t), quartet (q), and broad (br); chemical shifts (δ) are given in ppm and coupling constants (*J*) in hertz (Hz). ESI-MS spectra were performed by an Agilent 1100 Series LC/MSD spectrometer. All moisture-sensitive reactions were performed under argon atmosphere using oven-dried glassware and anhydrous solvents.

4.1.1. General procedure for the synthesis of the linear oligopeptides

The synthesis of linear oligopeptides was performed according to the solid phase approach using standard Fmoc methodology in a CEM Liberty Automated Microwave Peptide Synthesizer. Nα-Fmoc-protected amino acids, Wang-resin supported amino acids, HBTU, and trifluoroacetic acid were

purchased from Chem-Impex International (Illinois, USA). HOBt, DIEA, piperidine, acetic anhydride and solvents for peptide synthesis and HPLC were reagent grade and were acquired from Sigma Aldrich. The Fmoc-protected amino acids were added stepwise, according to the desired sequence. Each coupling reaction was accomplished using a 5-fold excess of amino acid at 0.1 mmol scales with HBTU and HOBt in the presence of DIEA. The Nα-Fmoc protecting groups was removed by treating the protected peptide resin with a 20% solution of piperidine in DMF (v/v) and the deprotection protocol was repeated after each coupling step. The *N*-terminal Fmoc group was removed as described above, and the acetylation of the free amine functionality, when required, was obtained by treating with a 20% solution of acetic anhydride in DMF (v/v). The peptide was released from the resin with TFA/*i*Pr_3SiH/H_2O (95:2.5:2.5) for 3 h. The resin was removed by filtration, and the crude peptide was recovered by precipitation with cold anhydrous diethyl ether to give a white powder.

4.1.2. General procedure for the cyclization of peptides

The appropriate linear sequence was dissolved in the minimum amount of dry DMF and then diluted with dry DCM. This solution was added dropwise to a mixture of HBTU (4 eq), HOBt (4 eq) and DIPEA (10 eq) in dry DCM, in order to have a solution with a final concentration of 10^{-5} M. The reaction was stirred at 25 °C under N_2 atmosphere for 12 h. Solvent was removed under reduced pressure and the crude was purified by means of chromatography on aluminum oxide (from 100% $CHCl_3$ to MeOH/$CHCl_3$ 1:30). The cyclic peptides were obtained with yields ranging from 17 to 25%.

*4.1.3. Ac-L-V-P-P-P-P-I-V-P-Y-F-COOH (**2b**)*

The title compound was obtained following the general procedure for the synthesis of linear peptides. **^{1}H NMR** (300 MHz, CD_3OD) δ 7.32-7.16 (m, 5H), 7.03 (d, *J* = 8.4 Hz, 2H), 6.67 (d, *J* = 8.3 Hz, 2H), 4.75-4.57 (m, 4H), 4.57-4.30 (m, 6H), 4.22 (d, *J* = 7.5 Hz, 1H), 4.00-3.70 (m, 5H), 3.68-3.47 (m, 5H), 3.15 (dd, *J* = 14.0, 5.5 Hz, 1H), 3.09-2.75 (m, 3H), 2.41-2.16 (m, 4H), 2.16-1.74 (m, 22H), 1.72-1.47 (m, 4H), 1.24-1.08 (m, 1H), 1.08-0.74 (m, 24H); **ESI-MS** *m/z* 1303 $[M+Na]^+$, 663 $[M+2Na]^{2+}/2$.

*4.1.4. Ac-L-V-P-P-P-P-I-V-P-Y-F-CONH$_2$ (**2a**)*

Compound **2b** (20 mg, 0.016 mmol) was suspended in dry MeCN (2.5 ml), then 2-ethoxy-1-ethoxycarbonyl-1,2-dihydroquinoline (EEDQ, 4 mg, 0.018 mmol) and NH_4HCO_3 (4 mg, 0.048 mmol) were added. The reaction was stirred at 25 °C under Ar atmosphere for 12 h. Solvent was removed under reduced pressure. The residue was taken up with a saturated solution of $NaHCO_3$ and the aqueous phase was extracted with DCM (3 x 10 mL). The combined organic layers were dried over Na_2SO_4, filtered and evaporated. The crude was purified by means of chromatography on silica gel (MeOH/$CHCl_3$ 1:10) to afford pure **2a** (35% yield) as a withe solid. **^{1}H NMR** (300 MHz, CD_3OD) δ 7.33-7.08 (m, 5H), 7.02 (d, *J* = 8.5 Hz, 2H), 6.66 (d, *J* = 11.6 Hz, 2H), 4.75-4.57 (m, 4H), 4.57-4.29 (m, 6H), 4.26-4.10 (m, 2H), 4.01-3.71 (m, 5H), 3.71-3.46 (m, 5H), 3.18-2.71 (m, 4H), 2.45-2.17 (m, 4H), 2.17-1.71 (m, 21H), 1.70-1.39 (m, 4H), 1.22-1.10 (m, 1H), 1.10-0.72 (m, 24H); **ESI-MS** *m/z* 1302 $[M+Na]^+$, 662 $[M+2Na]^{2+}/2$.

*4.1.5. Ac-P-P-I-V-P-Y-F-COOH (**3b**)*

The title compound was obtained following the general procedure for the synthesis of linear peptides. **^{1}H NMR** (300 MHz, CD_3OD) δ 7.30-7.12 (m, 5H), 7.03 (d, *J* = 8.5 Hz, 2H), 6.67 (d, *J* = 8.5 Hz, 2H), 4.68-4.56 (m, 2H), 4.55-4.40 (m, 3H), 4.38-4.26 (m, 1H), 4.22 (d, *J* = 7.8 Hz, 1H), 3.94-3.69 (m, 2H), 3.68-3.43 (m, 4H), 3.15 (dd, *J* = 13.9, 5.5 Hz, 1H), 3.09-2.83 (m, 3H), 2.25-1.72 (m, 17H), 1.64-1.46 (m, 1H), 1.24-1.10 (m, 1H), 1.02-0.79 (m, 12H); **ESI-MS** *m/z* 897 $[M+Na]^+$.

*4.1.5. Ac-P-P-I-V-P-Y-F-CON(Me)$_2$ (**3a**)*

To a solution of **3b** (20 mg, 0.022 mmol) in dry DCM (5 mL) cooled to 0 °C, EDCI (5 mg, 0.024 mmol), HOBt (4 mg, 0.024 mmol) and DIPEA (10 µL, 0.066 mmol) were added and the mixture was stirred under Ar atmosphere for 1 h. Then, a solution of dimethylamine hydrochloride in dry DCM (2.5 mL) and DIPEA (5 µL, 0.022 mmol) was added and the reaction was stirred at 25 °C for 12 h. Then a

saturated solution of $NaHCO_3$ was added and the aqueous phase was extracted with DCM (3 x 10 mL). The combined organic layers were dried over Na_2SO_4, filtered and evaporated. The crude was purified by means of chromatography on aluminum oxide (5% MeOH in $CHCl_3$) to afford pure **3a** (53% yield) as a white solid. **^{1}H NMR** (300 MHz, CD_3OD) δ 7.35-7.12 (m, 5H), 7.01 (d, *J* = 8.4 Hz, 2H), 6.66 (d, *J* = 8.3 Hz, 2H), 4.69-4.57 (m, 1H), 4.57-4.27 (m, 4H), 4.20 (d, *J* = 7.8 Hz, 1H), 4.01-3.71 (m, 4H), 3.69-3.47 (m, 4H), 3.13-2.72 (m, 8H), 2.34-1.68 (m, 18H), 1.57 (dd, *J* = 13.5, 7.3 Hz, 1H), 1.24-1.08 (m, 1H), 1.07-0.75 (m, 12H); **ESI-MS** *m/z* 902 $[M+H]^+$, 924 $[M+Na]^+$.

*4.1.6. Ac-V-P-P-P-P-I-CONH$_2$ (**4**)*

The title compound was obtained following the general procedure for the synthesis of linear peptides. Then, the free carboxylic terminus was converted into the corresponding primary amide following the same procedure reported for **2a**. The crude was purified by means of chromatography on aluminum oxide (5% MeOH in $CHCl_3$) to afford pure **4** (26% yield) as a withe solid. **^{1}H NMR** (300 MHz, $CDCl_3$) δ 7.44 (d, *J* = 9.0 Hz, 1H), 6.78 (br s, 1H), 6.22-6.02 (m, 2H), 4.81-4.52 (m, 4H), 4.39-4.07 (m, 4H), 3.92-3.38 (m, 8H), 2.65-2.39 (m, 1H), 2.33-1.80 (m, 18H), 1.59-1.36 (m, 2H), 1.06-0.76 (m, 12H); **ESI-MS** *m/z* 683 $[M+Na]^+$.

*4.1.7. NH$_2$(CH$_2$)$_3$CO-P-P-I-V-P-Y-F-COOH (**6a**)*

The title compound was obtained following the general procedure for the synthesis of linear peptides. **^{1}H NMR** (400 MHz, CD_3OD) δ 7.25-7.18 (m, 5H), 7.02 (d, *J* = 8.2 Hz, 2H), 6.67 (d, *J* = 8.2 Hz, 2H), 4.64-4.40 (m, 5H), 4.34 (m, 1H), 4.18 (t, *J* = 7.8 Hz, 1H), 3.84-3.70 (m, 2H), 3.66-3.45 (m, 4H), 3.13 (m, 1H), 3.02-2.86 (m, 5H), 2.60-2.40 (m, 2H), 2.25-1.70 (m, 16H), 1.60-1.45 (m, 1H), 1.14 (m, 1H), 0.95-0.85 (m, 12H); **ESI-MS** *m/z* 939 $[M+Na]^+$, 481 $[M+2Na]^{2+}/2$, 470 $[M+H+Na]^{2+}/2$.

*4.1.8. NH$_2$(CH$_2$)$_3$CO-P-P-I-V-G-Y-F-COOH (**6b**)*

The title compound was obtained following the general procedure for the synthesis of linear peptides. **^{1}H NMR** (400 MHz, CD_3OD) δ 7.20 (m, 5H), 6.98 (d, *J* = 8.4 Hz, 2H), 6.64 (d, *J* = 8.4 Hz, 2H), 4.60-

4.45 (m, 4H), 4.20 (d, *J* = 8.0 Hz, 1H), 4.11 (d, *J* = 7.2 Hz, 1H), 3.90-3.70 (m, 2H), 3.65-3.50 (m, 4H), 3.17 (m, 1H), 2.97 (m, 4H), 2.74 (m, 1H), 2.55-2.45 (m, 2H), 2.25-1.78 (m, 12H), 1.55-1.45 (m, 1H), 1.25-1.10 (m, 1H), 0.93-0.82 (m, 12H); **ESI-MS** *m/z* 878 $[M+H]^+$, 900 $[M+Na]^+$.

*4.1.9. $NH_2(CH_2)_2CO$-P-P-I-V-G-Y-F-COOH (**6c**)*

The title compound was obtained following the general procedure for the synthesis of linear peptides. **^{1}H NMR** (400 MHz, D_2O) δ 7.18 (m, 3H), 7.06 (d, *J* = 7.0 Hz, 2H), 6.92 (d, *J* = 8.2 Hz, 2H), 6.66 (d, *J* = 8.2 Hz, 2H), 4.56 (m, 1H), 4.41 (d, *J* = 7.1 Hz, 1H), 4.30 (m, 3H), 4.15 (t, *J* = 6.4 Hz, 1H), 3.99 (d, *J* = 8.5 Hz, 1H), 3.68 (m, 2H), 3.48 (m, 4H), 3.10 (m, 2H), 2.95-2.85 (m, 1H), 2.83-2.66 (m, 5H), 2.22-1.56 (m, 14H), 1.35 (m, 1H), 1.05 (m, 1H), 0.78-0.69 (m, 12H); **ESI-MS** *m/z* 904 $[M+H]^+$, 464 $[M+Na+H]^{2+}/2$, 453 $[M+2H]^{2+}/2$.

*4.1.10. NH_2-G-P-P-I-V-G-Y-F-COOH (**6d**)*

The title compound was obtained following the general procedure for the synthesis of linear peptides. **^{1}H NMR** (400 MHz, D_2O) δ 7.19 (m, 3H), 7.14 (d, *J* = 6.9 Hz, 2H), 7.06 (d, *J* = 6.9 Hz, 2H), 6.93 (d, *J* = 8.5 Hz, 2H), 6.67 (d, *J* = 8.3 Hz, 2H), 4.33 (m, 3H), 4.17 (t, *J* = 8.3 Hz, 1H), 3.99 (t, *J* = 7.8 Hz, 1H), 3.84 (s, 2H), 3.65 (m, 2H), 3.55-3.42 (m, 4H), 2.98-2.78 (m, 4H), 1.91-1.62 (m, 14H), 1.41-1.29 (m, 1H), 1.15-1.01 (m, 1H), 0,75 (m, 12H); **ESI-MS** *m/z* 911 $[M+Na]^+$, 889 $[M+H]^+$.

*4.1.11. $NH_2(CH_2)_3CO$-P-P-I-V-3,4-dehydro–(L)-proline-Y-F-COOH (**6e**)*

The title compound was obtained following the general procedure for the synthesis of linear peptides. **^{1}H NMR** (300 MHz, CD_3OD) δ 7.41-7.06 (m, 5H), 7.02 (d, *J* = 8.1 Hz, 2H), 6.66 (d, *J* = 6.8 Hz, 2H), 6.08-5.88 (m, 1H), 5.80-5.65 (m, 1H), 5.11-4.99 (m, 1H), 4.75-4.33 (m, 6H), 4.33-3.99 (m, 2H), 3.86-3.46 (m, 6H), 3.09 -2.79 (m, 5H), 2.62-2.41 (m, 2H), 2.29-1.63 (m, 12H), 1.63-1.39 (m, 1H), 1.04-0.72 (m, 12H); **ESI-MS** *m/z* 916 $[M+H]^+$, 938 $[M+Na]^+$, 470 $[M+H+Na]^{2+}/2$.

*4.1.12. Compound (**5a**)*

The title compound was obtained following the general procedure for the cyclization of linear peptides. **^{1}H NMR** (400 MHz, CD_3OD) δ 7.32-7.10 (m, 5H), 6.88-6.77 (m, 2H), 6.65 (m, 2H), 4.70-4.30 (m, 4H), 4.21 (m, 1H), 4,13 (m, 1H), 3.95 (m, 1H), 3.81-3.45 (m, 6H), 3.12-2.80 (m, 5H), 2.73 (m, 1H), 2.45-1.50 (m, 18H), 1.40-1.20 (m, 2H), 1.05-0.85 (m, 12 H); **ESI-MS** *m/z* 921 $[M+Na]^+$, 899 $[M+H]^+$.

*4.1.13. Compound (**5b**)*

The title compound was obtained following the general procedure for the cyclization of linear peptides. **^{1}H NMR** (400 MHz, CD_3OD) δ 7.37 (m, 1H), 7.26-7.16 (m, 6H), 6.94 (d, *J* = 8.3 Hz, 2H), 6.63 (m, 1H), 4.52-4.08 (m, 4H), 4.07-3.96 (m, 3H), 3.96-3.64 (m, 1H), 3.61-3.40 (m, 4H), 3.18 (m, 2H), 2.86 (m, 4H), 2.27-1.78 (m, 14H), 1.35-1.15 (m, 2H), 0.97 (m, 12H); **ESI-MS** *m/z* 883 $[M+Na]^+$, 860 $[M+H]^+$.

*4.1.14. Compound (**5c**)*

The title compound was obtained following the general procedure for the cyclization of linear peptides. **^{1}H NMR** (400 MHz, CD_3OD) δ 7.26-7.14 (m, 6H), 6.69 (m, 2H), 6.63-6.56 (m, 2H), 4.57-4.10 (m, 7H), 3.74-3.43 (m, 8H), 2.90-2.53 (m, 4H), 2.26 (m, 2H), 2.08-1.50 (m, 15H), 1.35 (m, 1H), 1.10-0.99 (m, 1H), 0.98-0.82 (m, 12H); **ESI-MS** *m/z* 907 $[M+Na]^+$.

*4.1.15. Compound (**5d**)*

The title compound was obtained following the general procedure for the cyclization of linear peptides. **^{1}H NMR** (400 MHz, CD_3OD) δ 7.30-7.18 (m, 6H), 6.60 (d, *J* = 8.4 Hz, 2H), 6,54 (d, *J* = 8.6 Hz, 2H), 4.64-4.55 (m, 2H), 4.37 (m, 2H), 4.03 (m, 1H), 3.96 (m, 1H), 3.90-3.79 (m, 2H), 3.66 (m, 1H), 3.46 (m, 6H), 2.90 (m, 2H), 2.55-2.45 (m, 2H), 2.19-1.78 (m, 14H), 1.55-1.45 (m, 2H), 1.25-1.15 (m, 1H), 0.96-0.80 (m, 12H); **ESI-MS** *m/z* 893 $[M+Na]^+$.

*4.1.16. Compound (**5e**)*

The title compound was obtained following the general procedure for the cyclization of linear peptides. **^{1}H NMR** (300 MHz, CD_3OD) δ 7.45-7.09 (m, 5H), 7.09-6.81 (m, 3H), 6.67 (d, *J* = 8.5 Hz, 2H), 6.04

(d, *J* = 6.7 Hz, 1H), 5.47 (d, *J* = 6.4 Hz, 1H), 5.24-5.07 (m, 1H), 4.65-4.33 (m, 4H), 4.33-4.02 (m, 2H), 3.77-3.42 (m, 6H), 3.12-2.63 (m, 6H), 2.47-1.42 (m, 16H), 1.08-0.66 (m, 12H); **ESI-MS** *m/z* 898 $[M+H]^+$, 920 $[M+Na]^+$.

*4.1.17. (4S)-1-tert-Butoxycarbonyl-4-iodo-(L)-proline methyl ester (**8**)*

To a solution of **7** (5.5 g, 22.7 mmol) in dry THF (50 mL), PPh_3 (9.0 g, 34.0 mmol) and MeI (1.7 mL, 27.1 mmol) were added and the mixture was cooled to 0 °C before adding DIAD (5.4 mL, 27.4 mmol) dropwise. The reaction was stirred at 25 °C under Ar atmosphere for 4 h. The off-white solid was filtered off and solvent was removed under reduced pressure. The crude was purified by means of flash chromatography (ethyl acetate/petroleum ether from 1:20 to 1:6) to afford pure compound **8** (55% yield) as slightly yellow oil. **^{1}H NMR** ($CDCl_3$, 300 MHz) 4.26 (dt, *J* = 24.1, 7.8 Hz, 1H), 4.15-3.95 (m, 2H), 3.74 (s, 3H), 3.70-3.57 (m, 1H), 2.87 (m, 1H), 2.42-2.21 (m, 1H), 1.42 (d, *J* = 15.6 Hz, 9H); **ESI-MS** *m/z* 356 $[M+H]^+$.

*4.1.18. 3,4-Dehydro-1-tert-butoxycarbonyl-(L)-proline methyl ester (**9**)*

To a solution of **8** (5.0 g, 14.9 mmol) in dry toluene (30 mL), DBU (2.7 g, 17.9 mmol) was added and the mixture was stirred at 85 °C for 3 h and then 12 h at 25 °C under At atmosphere. The slightly yellow precipitate was filtered off and toluene was removed under reduced pressure. The crude was purified by means of flash chromatography (ethyl acetate/petroleum ether 1:10) to afford pure compound **9** (78% yield) as a transparent oil. **^{1}H NMR** ($CDCl_3$, 300 MHz) ^{1}H NMR (300 MHz, $CDCl_3$) δ 6.05-5.89 (m, 1H), 5.79-5.65 (m, 1H), 5.09-4.91 (m, 1H), 4.35-4.12 (m, 2H), 3.73 (s, 3H), 1.46 (m, 9H); **ESI-MS** *m/z* 250 $[M+Na]^+$.

*4.1.19. 3,4-Dehydro-(L)-proline methyl ester hydrochloride salt (**10**)*

To a solution of **9** (100 mg, 0.4 mmol) in MeOH (5 mL), a solution of AcCl (710 µL) in MeOH (10 mL) was added and volatiles were removed under reduced pressure. The procedure was repeated until complete consumption of the starting material. No further purification was needed (quantitative yield).

^{1}H NMR (CD_3OD, 300 MHz) δ 6.16-6.06 (m, 1H), 6.06-5.98 (m, 1H), 5.26-5.18 (m, 1H), 4.28-4.09 (m, 2H), 3.86 (s, 3H); **ESI-MS** *m/z* 128 $[M+H]^+$.

*4.1.20. 3,4-Dehydro-1-tert-butoxycarbonyl-(L)-proline (**12**)*

To a solution of **9** (1.0 g, 4.4 mmol) in a 1:1 mixture of MeOH (10 mL) and THF (10 mL), a solution of LiOH (210 mg, 8.8 mmol) in water (10 mL) was added and the reaction was stirred at 25 °C under Ar atmosphere for 2 h. Volatilities were removed under reduced pressure and water was added. The aqueous phase was washed with ethyl acetate, acidified until pH = 2 with 1 N HCl, and extracted with ethyl acetate (3 x 10 mL). The combined organic layers were dried over Na_2SO_4, filtered and evaporated. Pure title compound was used in the following step without any further purification. **^{1}H NMR** (300 MHz, DMSO-d_6), δ 6.02-5.97 (m, 1H), 5.80-5.76 (m, 1H), 4.80-4.70 (m, 1H), 4.04-3.97 (m, 2H), 1.35 (s, 9H); **ESI-MS** *m/z* 212 $[M-H]^-$.

*4.1.21. 3,4-Dehydro-(L)-proline trifluoroacetate salt (**13**)*

To a solution of **12** (850 mg, 4.0 mmol) in dry DCM (20 mL), TFA (2 mL) was added and the reaction was stirred at 25 °C under Ar atmosphere for 2 h. Volatiles were removed under reduced pressure to afford pure title compound (quantitative yield) as a white solid. **^{1}H NMR** (300 MHz, D_2O), δ 5.95-5.90 (m, 1H), 5.85-5.80 (m, 1H), 5.10-4.95 (m, 1H), 4.11-3.98 (m, 2H); **ESI-MS** *m/z* 113 $[M-H]^-$.

*4.1.22. 3,4-Dehydro-1-(9-fluorenylmethoxycarbonyl)-(L)-proline (**14**)*

To a stirred solution of compound **13** (450 mg, 2.0 mmol) in Na_2CO_3 10 % solution (10 mL), a solution of 9-fluorenylmethyl chloroformate (520 mg, 2.0 mmol) in 1,4-dioxane (10 mL) was added the reaction was stirred at 25 °C for 4 h. Volatiles were removed under reduced pressure and the aqueous pahse was washed with Et_2O (2 x 10 mL), acidified till pH = 2 with 1 N HCl, and extracted with EtOAc (3 x 10 mL). The combined organic layers were dried over Na_2SO_4, filtered and evaporated. No further

purification was needed (76% yield). **^{1}H NMR** (300 MHz, $CDCl_3$), δ 9.65 (br s, 1H), 7.74 (d, *J* = 7,4 Hz, 1H), 7.69 (d, *J* = 7,2 Hz, 1H), 7.60-7.52 (m, 2H), 7.40-7.24 (m, 4H), 6.00-5.90 (m, 1H), 5.85-5.79 (m, 1H) 5.15-4.90 (m, 1H), 4.58-4.49 (m, 1H), 4.43-4.39 (m, 1H), 4.369-4.24 (m, 2H), 4.15-4.04 (m, 1H); **ESI-MS** *m/z* 334 $[M\text{-H}]^-$.

*4.1.23. (2-(2-Azidoethoxy)ethyl) tert-butoxycarbonylamine (**16**)*

Compound **15** (1.4 g, 9.0 mmol) was dissolved in MeOH (25 mL) and the solution was degassed several times with Ar before adding a catalytic amount of Pd/C 10%. The atmosphere was filled with H_2 and the reaction was stirred 8 h at 25 °C. The mixture was filtered and the solvent was removed under reduced pressure. The crude (1.1 g, 8.5 mmol) was dissolved in dry DCM (30 mL), then di-*tert*-butyl dicarbonate (2.2 g, 10.2 mmol) and TEA (3.0 mL, 21.3 mmol) were added. The reaction was stirred at 25 °C under Ar atmosphere for 12 h. Solvent was removed under reduced pressure. The crude was purified by means of chromatography on silica gel (ethyl acetate /petroleum ether 1:10) to afford title compound as a transparent oil (85% yield over 2-steps). **^{1}H NMR** (300 MHz, $CDCl_3$) δ 4.90 (br s, 1H), 3.64 (t, *J* = 4.9 Hz, 2H), 3.54 (t, *J* = 5.1 Hz, 2H), 3.45-3.22 (m, 4H), 1.44 (s, 9H); **ESI-MS** *m/z* 243 $[M\text{+Na}]^+$.

*4.1.24. (2-(2-Aminoethoxy)ethyl)-tert-butoxycarbonylamine (**17**)*

Compound **16** (1.7 g, 7.7 mmol) was dissolved in MeOH (25 mL) and the solution was degassed several times with Ar before adding a catalytic amount of Pd/C 10%. The atmosphere was filled with H_2 and the reaction was stirred 8 h at 25 °C. The mixture was filtered and the solvent was removed under reduced pressure. No further purification was needed (quantitative yield). **^{1}H NMR** (300 MHz, $CDCl_3$) δ 5.08 (br s, 1H), 3.66-3.47 (m, 4H), 3.37-3.22 (m, 2H), 3.22-3.10 (m, 2H), 3.02-2.84 (m, 2H), 1.43 (s, 9H); **ESI-MS** *m/z* 205 $[M\text{+H}]^+$, 227 $[M\text{+Na}]^+$.

*4.1.25. (2-(2-(tert-Butoxycarbonyl)aminoethoxy)-ethylaminocarbonyl)-(L)-isoleucine benzyl ester (**18**)*

(2S,3S)-Benzyl-2-isocyanato-3-methylpentanoate. To a stirred solution of (*L*)-Ile-OBn (205 mg, 0.93 mmol) in DCM (10 mL) cooled to 0 °C, a saturated solution of $NaHCO_3$ (10 mL) was added and the suspension was vigorously stirred for 5 min. Then, a 20% solution of phosgene in toluene (1.0 mL, 1.86 mmol) was added and the reaction was stirred for further 15 min at 25 °C. The two layers were separated and the aqueous phase was extracted with DCM (3 x 10 mL). The combined organic layers were dried over Na_2SO_4, filtered and evaporated. **^{1}H NMR** (300 MHz, $CDCl_3$) δ 7.41-7.32 (m, 5H), 5.22 (q, *J* = 12.1 Hz, 2H), 4.15-3.94 (m, 1H), 2.01-1.87 (m, 1H), 1.53-1.09 (m, 2H), 1.03-0.72 (m, 6H); **ESI-MS** *m/z* 248 $[M+H]^+$.

To a stirred solution of the previously synthesized isocyanate (225 mg, 0.93 mmol) and **17** (190 mg, 0.93 mmol) in dry THF (10 mL), TEA (150 µL, 1.02 mmol) was added and the mixture was stirred at 25 °C under Ar atmosphere for 12 h. Solvent was removed under reduced pressure. The crude was purified by means of flash chromatography on silica gel (ethylacetate/petroleum ether 1:1) to afford title compound (62 % yield) as an off-white solid. **^{1}H NMR** (300 MHz, $CDCl_3$) δ 5.35 (br s, 1H), 5.16 (qd, *J* = 12.3, 2.2 Hz, 2H), 5.05 (br s, 1H), 4.55 (ddd, *J* = 38.2, 9.0, 4.4 Hz, 1H), 3.66-3.42 (m, 4H), 3.42-3.17 (m, 4H), 2.00-1.78 (m, 1H), 1.45 (s, 9H), 1.23-1.04 (m, 1H), 0.98-0.72 (m, 6H); **ESI-MS** *m/z* 452 $[M+H]^+$.

*4.1.26. (2-(2-(tert-Butoxycarbonyl)aminoethoxy)-ethylaminocarbonyl)-(L)-isoleucine (**19**)*

Starting from **18** (250 mg, 0.55 mmol), the title compound was obtained following the same procedure reported for **17** (quantitative yield). The compound was used in the following steps without further purification. **^{1}H NMR** (300 MHz, $CDCl_3$) δ 8.57 (br s, 1H), 5.97 (br s, 2H), 5.38 (br s, 1H), 4.65-4.27 (m, 1H), 3.61-3.36 (m, 4H), 3.36-2.98 (m, 4H), 2.08-1.78 (m, 1H), 1.42 (s, 9H), 1.24-1.03 (m, 1H), 1.01-0.75 (m, 6H); **ESI-MS** *m/z* 360 $[M-H]^-$.

*4.1.27. N-(tert-Butoxycarbonyl)-(L)-valine-(3,4-dehydro)-(L)-proline methyl ester (**20**)*

Starting from amine **10** (1.0 g, 4.6 mmol) and *N*-Boc-*L*-Valine (480 mg, 3.8 mmol), title compound was obtained following the same procedure reported for **3a**. The crude was purified by means of flash chromatography on silica gel (ethyl acetate/petroleum ether 1:10) to afford pure compound **20** (62% yield) as a white solid. **ESI-MS** *m/z* 327 $[M+H]^+$, 350 $[M+Na]^+$; **^{1}H NMR** (300 MHz, $CDCl_3$) δ 5.98 (d, *J* = 6.4 Hz, 1H), 5.82 (d, *J* = 4.0 Hz, 1H), 5.25 (br s, 1H), 5.15 (d, *J* = 9.8 Hz, 1H), 4.68-4.37 (m, 2H), 4.23 (q, *J* = 7.5 Hz, 1H), 3.72 (s, 3H), 2.15-1.94 (m, 1H), 1.42 (s, 9H), 1.05 (d, *J* = 6.8 Hz, 3H), 1.01-0.83 (m, 4H).

*4.1.28. N-(tert-Butoxycarbonyl)-(L)-valine-(3,4-dehydro)-(L)-proline (**21**)*

To a solution of **20** (700 mg, 2.2 mmol) in a 1:1 mixture of MeOH (5 mL) and THF (5 mL), a solution of LiOH (100 mg, 4.4 mmol) in water (5 mL) was added and the reaction was stirred at 25 °C under Ar atmosphere for 2 h. Volatiles were removed under reduced pressure and water was added. The aqueous phase was washed with ethyl acetate, acidified until pH = 2 with 1N HCl, and extracted with ethyl acetate (3 x 15 mL). The combined organic layers were dried over Na_2SO_4, filtered and evaporated. Pure title compound was used in the following step without any further purification. **ESI-MS** *m/z* 311 $[M-H]^-$.

*4.1.29. (L)-Valine-(3,4-dehydro)-(L)-proline-(O-benzyl)-(L)-tyrosine-(L)-phenylalanine methyl ester hydrochloride salt (**23**)*

Starting from acid **21** (500 mg, 1.6 mmol) and amine **22** (560 mg, 1.3 mmol), title compound was obtained following the same procedure reported for **3a**. The crude was purified by means of flash chromatography on silica gel (ethyl acetate/petroleum ether 1:2) to afford pure Boc-protected intermediate (53% yield) as a white solid. **^{1}H NMR** (300 MHz, $CDCl_3$) δ 7.30-7.13 (m, 4H), 7.13-7.00 (m, 4H), 6.97-6.78 (m, 4H), 6.69 (d, *J* = 8.3 Hz, 2H), 6.58 (d, *J* = 7.4 Hz, 1H), 6.08 (d, *J* = 7.5 Hz, 1H), 5.77 (d, *J* = 5.9 Hz, 1H), 5.65 (d, *J* = 5.8 Hz, 1H), 5.03-4.96 (m, 1H), 4.85 (s, 2H), 4.57 (q, *J* = 6.7 Hz,

1H), 4.47-4.29 (m, 2H), 4.23-3.98 (m, 2H), 3.49 (s, 3H), 2.99-2.68 (m, 4H), 1.73 (q, *J* = 6.6 Hz, 1H), 1.27 (s, 9H), 0.83-0.63 (m, 7H); **ESI-MS** *m/z* 727 $[M+H]^+$, 749 $[M+Na]^+$.

Pure amine **23** was obtained following the same procedure reported for **10** and was used in the following step without any further purification (quantitative yield). **ESI-MS** *m/z* 627 $[M+H]^+$, 649 $[M+Na]^+$.

*4.1.30. (2-(2-(tert-Butoxycarbonyl)aminoethoxy)-ethylaminocarbonyl)-(L)-isoleucine-(L)-valine-(3,4-dehydro)-(L)-proline-(O-benzyl)-(L)-tyrosine-(L)-phenylalanine methyl ester (**24**)*

Starting from acid **19** (200 mg, 0.55 mmol) and amine **23** (345 mg, 0.55 mmol), the title compound was obtained following the same procedure reported for **3a**. The crude was purified by means of flash chromatography on silica gel (ethyl acetate/ petroleum ether 1:1) to afford pure compound **24** (43% yield) as a white solid. **^{1}H NMR** (300 MHz, CD_3OD) δ 7.47-7.16 (m, 7H), 7.15-7.06 (m, 4H), 6.86 (d, *J* = 8.7 Hz, 2H), 5.97 (dd, *J* = 6.3, 1.8 Hz, 1H), 5.67 (dd, *J* = 6.0, 2.4 Hz, 1H), 5.16-5.05 (m, 1H), 5.01 (s, 2H), 4.73-4.28 (m, 6H), 4.16 (d, *J* = 6.9 Hz, 1H), 3.58 (s, 3H), 3.51-3.39 (m, 4H), 3.38-3.13 (m, 4H), 3.10-2.86 (m, 4H), 2.17-2.01 (m, 1H), 1.95-1.83 (m, 1H), 1.83-1.70 (m, 1H), 1.42 (s, 9H), 1.04-0.80 (m, 12H); **ESI-MS** *m/z* 497 $[M+H+Na]^{2+}/2$, 508 $[M+2Na]^{2+}/2$, 971 $[M+H]^+$, 993 $[M+Na]^+$.

*4.1.31. (2-(2-Aminoethoxy)-ethylaminocarbonyl)-(L)-isoleucine-(L)-valine-(3,4-dehydro)-(L)-proline-(O-benzyl)-(L)-tyrosine-(L)-phenylalanine (**6f**)*

(2-(2-(tert-Butoxycarbonyl)aminoethoxy)-ethylaminocarbonyl)-(L)-isoleucine-(L)-valine-(3,4-dehydro)-(L)-proline-(O-benzyl)-(L)-tyrosine-(L)-phenylalanine. Starting from compound **24**, the ester functionality was converted into the corresponding free acid following the same procedure reported for **21**. No further purification was needed (quantitative yield). **^{1}H NMR** (300 MHz, CD_3OD) δ 7.48-7.06 (m, 12H), 6.85 (d, *J* = 8.4 Hz, 2H), 5.97 (d, *J* = 4.9 Hz, 1H), 5.68 (d, *J* = 2.6 Hz, 1H), 5.14-5.04 (m, 1H), 5.01 (s, 2H), 4.75-4.28 (m, 6H), 4.13 (d, *J* = 6.9 Hz, 1H), 3.53-3.36 (m, 4H), 3.36-3.08 (m, 6H),

3.08-2.80 (m, 2H), 2.19-2.00 (m, 1H), 1.97-1.88 (m, 1H), 1.80-1.66 (m, 1H), 1.42 (s, 9H), 1.06-0.74 (m, 12H); **ESI-MS** *m/z* 490 $[M+H+Na]^{2+}/2$, 501 $[M+2Na]^{2+}/2$, 957 $[M+H]^{+}$, 979 $[M+Na]^{+}$.

The intermediate free acid was dissolved in dry DCM and TFA was added. The reaction was stirred at 25 °C under Ar atmosphere for 2 h. Volatiles were removed under reduced pressure to afford pure title compound (quantitative yield) as a white solid. **^{1}H NMR** (300 MHz, CD_3OD) δ 7.47-7.02 (m, 12H), 6.86 (d, *J* = 8.3 Hz, 2H), 6.00 (d, *J* = 5.1 Hz, 1H), 5.70 (d, *J* = 3.9 Hz, 1H), 5.12-5.06 (m, 1H), 5.02 (s, 2H), 4.76-4.25 (m, 6H), 4.13 (d, *J* = 6.8 Hz, 1H), 3.73-3.62 (m, 2H), 3.59-3.45 (m, 2H), 3.45-3.22 (m, 2H), 3.21-2.82 (m, 6H), 2.25-2.01 (m, 1H), 1.97-1.75 (m, 1H), 1.62-1.33 (m, 1H), 1.05-0.76 (m, 12H); **ESI-MS** *m/z* 451 $[M+2Na]^{2+}/2$, 857 $[M+H]^{+}$, 879 $[M+Na]^{+}$.

*4.1.32. Compound **5f***

Starting from compound **6f**, the tile compound was obtained following the general procedure for the cyclization of linear peptides. The crude was purified by means of chromatography on silica gel (methanol/ethyl acetate 1:10) to afford pure title compound as a white solid. **^{1}H NMR** (300 MHz, CD_3OD) δ 7.47-7.17 (m, 12H), 6.79 (d, *J* = 4.7 Hz, 2H), 6.07 (d, *J* = 6.3 Hz, 1H), 5.62 (d, *J* = 6.5 Hz, 1H), 5.03 (s, 2H), 4.97 (d, *J* = 2.4 Hz, 1H), 4.70-4.41 (m, 4H), 4.09-3.89 (m, 2H), 3.74-3.33 (m, 6H), 3.15-2.60 (m, 6H), 2.25-1.77 (m, 2H), 1.65-1.43 (m, 1H), 1.37-1.19 (m, 1H), 1.06-0.74 (m, 12H); **ESI-MS** *m/z* 839 $[M+H]^{+}$, 861 $[M+Na]^{+}$;

*4.1.33. Compound **5g***

Compound **5f** (5.0 mg, 0.0 mmol) was dissolved in dry DCM (2 mL) and the solution was cooled to -78 °C. Then, a 1 M solution of BCl_3 in DCM (30 µL, 0.0 mmol) was added and the mixture was warmed to 25 °C and stirred for 12 h under Ar atmosphere. Volatiles were removed under reduced pressure. The crude was purified by means of chromatography on silica gel (methanol/ethyl acetate 1:10) to afford pure title compound as a white solid (45% yield). **^{1}H NMR** (300 MHz, CD_3OD) δ 7.43-

7.11 (m, 7H), 6.73-6.54 (m, 2H), 6.10 (d, *J* = 6.3 Hz, 1H), 5.69 (d, *J* = 6.3 Hz, 1H), 5.04-4.93 (m, 1H), 4.72-4.41 (m, 4H), 4.11-3.91 (m, 2H), 3.73-3.37 (m, 6H), 3.05-2.59 (m, 6H), 2.38-1.79 (m, 3H), 1.67-1.46 (m, 1H), 1.11-0.72 (m, 12H); **ESI-MS** *m/z* 748 $[M+H]^+$, 770 $[M+Na]^+$, 786 $[M+K]^+$.

4.2. NMR Studies

4.2.1. NMR Samples preparation

Samples were prepared by dissolving 20 mg of peptide in 500 µL of D_2O (99,96% D, Merck) and d6-DMSO (99,90% D, Aldrich) for **2b** and **5a**, respectively. The same amount of **2b** were dissolved in H_2O (10% v/v D_2O) to observe labile protons. All NMR samples were stored at 277 K.

4.2.2. NMR data acquisition and processing

Two-dimensional NMR spectra were recorded at 277, 298 and 308 K on a Bruker DRX 600 spectrometer equipped with an *xyz* gradient unit and using a probe SEI (Selected Enhance Inverse).

One-dimensional (1D) NMR spectra were used for the analysis of temperature dependence of labile protons chemical shift by recording spectra at 277 K, 298 K, 300 K, 308 K, 313 K and 323 K and at 293 K, 298 K, 303 K, 313 K and 323 K for **2b** and **5a**, respectively.

2D ^{1}H NMR NOESY (relaxation delay 3 s, mixing time 400 ms), DQF-COSY and TOCSY (mixing time 200 ms) experiments were recorded in phase-sensitive mode. Spectral width was 7184 Hz, with F1=4096 and F2=256 complex points.

All spectra were processed with Bruker's *XWINNMR*© software and analysed using *Sparky 3.115 (*Goddard T. D., Kneller D. G., SPARKY 3, University of California, San Francisco).

4.2.3. Generation of restraints

Distance restraints and dihedral angle restraints. Distance restraints were derived from NOE peaks volumes. Initially, a set of simplified restraints was generated by qualitatively dividing the NOEs intensities in *small*, *medium* and *large* (rated with the range of 4.0-5.0 Å, 2.5-4.0 Å and 1.7-2.5 Å respectively).

Subsequently, the NOEs volumes were first integrated to intensities using *Sparky* and then the relaxation matrix was analysed using *CORMA/MARDIGRAS*[50] algorithms for discerning proton-proton distances. In this way it was possible to generate a more precise distance restraint list.

The $^{3}J_{HN\text{-}HA}$ coupling constant values were directly measured in 1D ^{1}H-spectra and used as restraints in molecular dynamics simulations, giving information on the φ dihedral angle (H, N, Cα, Hα).

4.2.4. Minimizations and Molecular Dynamics

All molecular dynamics simulations were performed using the *Amber 14* [21] suite of programs specifying the *ff99SB* force field[51].

The starting structures generated by using *xLEaP* module of *Amber 14*, were submitted to minimization and equilibration using a short molecular dynamics runs with no restraints applied. Minimizations and molecular dynamics were run using the *Sander* (Simulated Annealing with NMR-Derived Energy Restraints) module of *Amber 14*.

The MD run was performed in two parts. In the first part (2000 ps) $^{3}J_{HN\text{-}HA}$ restraints and a simplified set of distance restraints were applied, in order to gradually obtain roughly NMR-refined structures; implicit solvent and simulated annealing were used. In the second part (3000 ps) all the NMR distance restraints were applied. Implicit solvent and simulated annealing were applied in the first 1000ps, followed by a constant temperature run. The total length of the run was 5000 ps with steps of 1.0 fs.

4.3. Molecular Modelling

4.3.1. Computational Details

All calculations performed in this work were carried out on two Cooler Master Centurion 5 (Intel Core-i5 Quad CPU Q6600 @ 2.40 GHz) with Ubuntu 10.04 LTS (long-term support) operating system running Maestro 9.2 (Schrödinger, LLC, New York, NY, 2011), GOLD 5.2 (Cambridge

Crystallographic Data Center, CCDC, UK), and Autodock 4.2.6 via AutodockTools 4 (MGL tools 1.5.6)(http://autodock.scripps.edu/).[32]

4.3.2. Molecular Docking Studies

a) Ligand preparation. Three-dimensional structures of all compounds in this study were built by means of Maestro.[37] Molecular energy minimizations were performed by means of MacroModel[25] using the Optimized Potentials for Liquid Simulations-all atom (OPLS-AA) force field 2005.[52] The solvent effects are simulated using the analytical Generalized-Born/Surface-Area (GB/SA) model,[53] and no cutoff for nonbonded interactions was selected. Polak-Ribiere conjugate gradient (PRCG)[54] method with 1000 maximum iterations and 0.001 gradient convergence threshold was employed. The conformational searches were carried out by application of the MCMM (Monte Carlo Multiple Minimum) torsional sampling method, performing automatic setup with 21 kJ/mol (5.02 kcal/mol) in the energy window for saving structure and a 0.5 Å cutoff distance for redundant conformers. All compounds reported in this paper were treated by LigPrep application,[55] implemented in Maestro suite 2011, generating the most probable ionization state of any possible enantiomers and tautomers at cellular pH value (7 ± 0.5).

b) Protein preparation. The three-dimensional structure of the α/β-tubulin (PDB ID: 1JFF[56]) was taken from PDB and imported into Schrödinger Maestro molecular modeling environment.[37] The structure was submitted to protein preparation wizard implemented in Maestro suite 2011 (Protein Preparation Wizard workflow 2011; http://www.schrodinger.com/supportdocs/18/16). This protocol through a series of computational steps, allowed us to obtain a reasonable starting structure of the proteins for molecular docking calculations by a series of computational steps. In particular, we performed three steps to (1) add hydrogens, (2) optimize the orientation of hydroxyl groups, Asn, and Gln, and the protonation state of His, and (3) perform a constrained refinement with the impref utility,

setting the max RMSD of 0.30. The impref utility consists of a cycles of energy minimization based on the impact molecular mechanics engine and on the OPLS_2005 force field.[52]

c) Blind Docking. Blind Docking study was performed by means of Autodock by using Graphical User Interface program AutoDock Tools (ADT).[32] The protein and the ligand (**5a**) prepared as above specified were submitted to ADT in order to generate the structure files for Autodock in .pdbqt format. ADT assigned polar hydrogens, united atom Kollman charges, solvation parameters and fragmental volumes to the protein. AutoGrid was used for the preparation of the grid map using a grid box. The grid size was set to 105 × 75 × 65 xyz points with grid spacing of 1 Å and the grid center was designated at dimensions (x, y, and z): 18.303, -1.735 and 3.426. By using these parameters all the protein was considered for our blind docking calculation. During the docking procedure the protein was considered as rigid. Docking simulations of **5a** were carried out using the Lamarckian genetic algorithm and through a protocol with an initial population of 150 randomly placed individuals, a maximum number of 2,5 million energy evaluations. For the local search a maximum of 300 interactions was applied. The docked solutions comprised between -9.341 and -6.505 kcal/mol corresponding to an estimated affinity of 20-100 μM, were visualized as reported in Fig. 5.

c) Molecular Docking .Molecular Docking was carried out using GOLD 5.2 Genetic Optimization for Ligand Docking) software from Cambridge Crystallographic Data Center, UK, that uses the Genetic algorithm (GA)[33] running under Ubuntu 10.04 LTS OS. This method allows a partial flexibility of protein and full flexibility of ligand. For each of the 100 independent GA runs, a maximum number of 125000 GA operations were performed. The search efficiency values were set on 200% in order to increase the flexibility of the ligands docked. As reported in the gold user manual this setting of the parameter is recommended for large highly flexible ligands. The active site radius of 10Å was chosen from the center of the crystallized molecule. Default cutoff values of 2.5 Å (dH-X) for hydrogen bonds

and 4.0 Å for van der Waals distance were employed. When the top three solutions attained RMSD values within 1.5 Å, GA docking was terminated. The fitness functions ChemScore coupled to GoldScore for rescoring the docked solutions were evaluated. The interactions of the docked poses with the identified binding site were evaluated by ligand interaction diagram tool coupled to a contacts assessment performed by means of measurement tool implemented in Maestro suite.

d) Estimated free-binding energies. The Prime/MM-GBSA method implemented in Prime software[57] consists in computing the change between the free and the complex state of both the ligand and the protein after energy minimization. The technique was used on the docking complexes presented in Fig. 6A-C. The software was used to calculate the free-binding energy (ΔG_{bind}) as previously reported by us.[38-40, 43]

4.4. Biological Studies

4.4.1. Cell lines

Human promyelocytic leukaemia cells HL60 (ECACC), human T lymphocyte Jurkat cells and Epstein-Barr Virus (EBV)-immortalized B cells (EBV-B) were maintained at a density between 200,000-1,000,000 cell/mL at 37 °C with 5% CO_2 in RPMI-1640 media with GlutaMAX™ supplemented with 10% foetal bovine serum, 50 U/mL penicillin and 50 µg/mL streptomycin (Invitrogen, Carlsbad, CA, USA). The cells were treated at a density of 200,000 cells/mL.

The rat basophilic leukemia (RBL) cell line (RBL-2H3) kindly provided by M. De Bernard (Department of Biology, University of Padua, Padua, Italy) were maintained in Dulbecco's Modified Eagle's medium (DMEM) medium containing 10% FBS, 1% L-glutamine and 1% penicillin-streptomycin at 37 °C with 5% CO_2. Upon reaching 70-80% confluency, the cells were sub-cultured

using trypsin/EDTA. Prior to treating, the cells were seeded at a density of 50,000 cells/mL and cultured for 24 h.

Human breast carcinoma MCF-7 cells (ECACC) were maintained at 37 °C with 5% CO_2 in Minimum Essential Medium (MEM) with GlutaMAX™ supplemented with 1% non-essential amino acids, 10% foetal bovine serum, 50 U/mL penicillin and 50 μg/mL streptomycin (Invitrogen, Carlsbad, CA, USA). Upon reaching 70-80% confluency, the cells were sub-cultured using trypsin/EDTA. Prior to treating, the cells were seeded at a density of 50,000 cells/mL and cultured for 24 h.

A375 human malignant melanoma cell lines obtained from American Type Culture Collection (ATCC) and the 501Mel cell lines obtained from surgically removed metastases in melanoma patients at the National Cancer Institute, Milan, Italy were maintained in DMEM medium containing 10% FBS, 1% L-glutamine and 1% penicillin-streptomycin at 37 °C with 5% CO_2. The cells were treated at a density of 150,000 cells/mL and culture for up to 72 h.

4.4.2. Cell treatments with the tested compounds, and analysis of apopotosis.

Cells (10^6/sample) were treated with 50 μM cyclic (**5a-g**) or linear (**2a,b** and **6a-f**) peptides for 24 h. Control samples were treated with vehicle (0.1% DMSO). Alternatively cells were treated with 1, 10, 25, 50 and 100 μM **5a,c,d,f** and for different time points up to 72 h. Apoptosis was assessed by measuring ''sub-G_0/G_1'' DNA content, dissipation of the mitochondrial membrane potential and phosphatidylserine exposure to the cell surface using flow cytometry.

Flow cytometry was carried out using a FACScan flow cytometer (Becton-Dickinson, San Jose, CA, USA) equipped with a 15-mW 488 nm argon ion laser. The green (FL1) and red (FL2) fluorescence data were collected through a 530/30 and a 585/42 band pass filter, respectively. Data acquisition was performed using CellQuest software. Data were analyzed and plotted using Flowjo.

Cell cycle distribution was quantified by flow cytometric analysis of propidium iodide (PI Invitrogen UK) stained cells. Briefly, cells treated as described in "Cells treatments" were fixed and permeabilized with 70% ethanol overnight at 4 °C and incubated with 100 µg RNAse and 20 µg/mL PI (Sigma) for 30 min. Samples were analyzed in a FACScan flow cytometer (Becton Dickinson, San Jose, CA) using CellQuest software. Doublets were excluded and 20.000 events were acquired for each sample.

Mitochondrial membrane potential was measured using the fluorescent probe, TMRM (Molecular Probes Europe BV). Cells (10^6/sample) were suspended in 200 mL RPMI 1640 w/o phenol Red (Invitrogen srl) added with 25 mM Hepes pH 7.4 and 200 nM TMRM and incubated for 20 min at 37 °C. Cells were then diluted to 1 mL with RPMI 1640 w/o phenol Red added with 25 mM Hepes pH 7.4 and subjected to flow cytometric analysis.

Phosphatidylserine exposure to the cell surface was quantitated by flow cytometric analysis of cells stained with FITC-conjugated Annexin V and 50 µg/mL PI using Annexin V apoptosis Detection kit FITC (eBioscience, San Diego, CA).

4.4.3. Cellular lysates.

HL60 cells (5.0 x 10^7/ sample) were treated with vehicle or with **2b** and **5a** for 6, 12, 24 and 48 h at 37 °C in a humidified atmosphere containing 5% CO_2 cells were centrifuged at 1000 rcf for 5 min at rt and the culture medium was carefully removed. The pellet was washed with cold PBS, and cells were collected by centrifugation. Then the supernatant was carefully removed. 1 mL of cold radioimmunoprecipitation assay (RIPA) buffer (Sigma-Aldrich, Germany) with freshly added protease inhibitor mixture and 1 mM sodium orthovanadate was added and cells were suspended in RIPA buffer and incubated on ice for 30 min. Cells were afterwards centrifuged at 10.000 rcf for 10 min at 4 °C. The pellets were then discarded and the supernatants transferred to new microcentrifuge tubes and analysed. The sample was tested in triplicate for each incubation time (6, 12, 24 and 48 h).

4.4.4. Confocal microscopy

HL-60 cells were seeded on poly-*L*-Lysine-coated slides, treated with 50 μM of the tested compounds or vehicle (0.1% DMSO) for 15 min at rt and fixed for 20 min in 4% PFA.

RBL-2H3 cells were seeded on uncoated slides and treated with 50 μM of the tested compounds, 0.5 μM of **1** or vehicle (0.1% DMSO) for 16 h. Cells were fixed and permeabilized for 10 min at -20 °C in methanol and stained overnight at 4 °C with anti-tubulin antibody, followed by Alexa-Fluor 488 goat anti-mouse secondary antibody.

Confocal laser-scanning microscopy analyses were carried out on a Zeiss LSM700 (Zeiss, Oberkochen, Germany).

Acknowledgments.

Authors thank Regione Toscana (Bando Salute) and Ministry of Education, University and Research, PRIN, n. 2010C2LKKJ_001.

References

[1] D.G. Kingston, Tubulin-interactive natural products as anticancer agents, J. Nat. Prod. 72 (2009) 507-515.
[2] M.A. Jordan, L. Wilson, Microtubules as a target for anticancer drugs, Nat. Rev. Cancer, 4 (2004) 253-265.
[3] M.M. Mc Gee, S. Gemma, S. Butini, A. Ramunno, D.M. Zisterer, C. Fattorusso, B. Catalanotti, G. Kukreja, I. Fiorini, C. Pisano, C. Cucco, E. Novellino, V. Nacci, D.C. Williams, G. Campiani, Pyrrolo[1,5]benzoxa(thia)zepines as a new class of potent apoptotic agents. Biological studies and identification of an intracellular location of their drug target, J. Med. Chem. 48 (2005) 4367-4377.
[4] J.C. Lennon, S.A. Bright, E. Carroll, S. Butini, G. Campiani, A. O'Meara, D.C. Williams, D.M. Zisterer, The novel pyrrolo-1,5-benzoxazepine, PBOX-6, synergistically enhances the apoptotic effects of carboplatin in drug sensitive and multidrug resistant neuroblastoma cells, Biochem. Pharmacol. 87 (2014) 611-624.
[5] A.M. McElligott, E.N. Maginn, L.M. Greene, S. McGuckin, A. Hayat, P.V. Browne, S. Butini, G. Campiani, M.A. Catherwood, E. Vandenberghe, D.C. Williams, D.M. Zisterer, M. Lawler, The novel tubulin-targeting agent pyrrolo-1,5-benzoxazepine-15 induces apoptosis in poor prognostic subgroups of chronic lymphocytic leukemia, Cancer Res. 69 (2009) 8366-8375.
[6] J.M. Mulligan, L.M. Greene, S. Cloonan, M.M. Mc Gee, V. Onnis, G. Campiani, C. Fattorusso, M. Lawler, D.C. Williams, D.M. Zisterer, Identification of tubulin as the molecular target of proapoptotic pyrrolo-1,5-benzoxazepines, Mol. Pharmacol. 70 (2006) 60-70.
[7] M.A. Jordan, K. Kamath, How do microtubule-targeted drugs work? An overview, Curr. Cancer Drug Targets, 7 (2007) 730-742.
[8] K.H. Altmann, J. Gertsch, Anticancer drugs from nature--natural products as a unique source of new microtubule-stabilizing agents, Natural product reports, 24 (2007) 327-357.
[9] P.B. Schiff, J. Fant, S.B. Horwitz, Promotion of microtubule assembly in vitro by taxol, Nature, 277 (1979) 665-667.
[10] J.G. Chen, S.B. Horwitz, Differential mitotic responses to microtubule-stabilizing and -destabilizing drugs, Cancer Res. 62 (2002) 1935-1938.
[11] J.G. Chen, C.P. Yang, M. Cammer, S.B. Horwitz, Gene expression and mitotic exit induced by microtubule-stabilizing drugs, Cancer Res. 63 (2003) 7891-7899.
[12] M.A. Jordan, R.J. Toso, D. Thrower, L. Wilson, Mechanism of mitotic block and inhibition of cell proliferation by taxol at low concentrations, Proc. Natl. Acad. Sci. USA, 90 (1993) 9552-9556.
[13] C. Ferlini, L. Cicchillitti, G. Raspaglio, S. Bartollino, S. Cimitan, C. Bertucci, S. Mozzetti, D. Gallo, M. Persico, C. Fattorusso, G. Campiani, G. Scambia, Paclitaxel directly binds to Bcl-2 and functionally mimics activity of Nur77, Cancer Res. 69 (2009) 6906-6914.
[14] V.L. Schuster, Y. Chi, A.S. Wasmuth, R.S. Pottorf, G.L. Olson, Preparation of diaminotriazine derivatives for use as prostaglandin transporter inhibitors, in: WO2010US02555, 2011.
[15] N. Shangguan, M. Joullie, A Copper-Carbodiimide Approach to the Phomopsin Tripeptide Side Chain, Tetrahedron Lett. 50 (2009) 6748-6750.
[16] J. Maupetit, P. Derreumaux, P. Tuffery, PEP-FOLD: an online resource for de novo peptide structure prediction, Nucleic Acids Res. 37 (2009) W498-503.
[17] A.C. Camproux, R. Gautier, P. Tuffery, A hidden markov model derived structural alphabet for proteins, J. Mol. Biol. 339 (2004) 591-605.
[18] H. Kaur, A. Garg, G.P. Raghava, PEPstr: a de novo method for tertiary structure prediction of small bioactive peptides, Protein Pept. Lett. 14 (2007) 626-631.
[19] D.T. Jones, Protein secondary structure prediction based on position-specific scoring matrices, J. Mol. Biol. 292 (1999) 195-202.

[20] H. Kaur, G.P. Raghava, A neural network method for prediction of beta-turn types in proteins using evolutionary information, Bioinformatics, 20 (2004) 2751-2758.
[21] D.A. Case, J.T. Berryman, R.M. Betz, D.S. Cerutti, T.E.I. Cheatham, T.A. Darden, R.E. Duke, T.J. Giese, H. Gohlke, A.W. Goetz, N. Homeyer, S. Izadi, P. Janowski, J. Kaus, A. Kovalenko, T.S. Lee, S. LeGrand, P. Li, T. Luchko, R. Luo, B. Madej, K.M. Merz, G. Monard, P. Needham, H. Nguyen, H.T. Nguyen, I. Omelyan, A. Onufriev, D.R. Roe, A. Roitberg, R. Salomon-Ferrer, C.L. Simmerling, W. Smith, J. Swails, R.C. Walker, J. Wang, R.M. Wolf, X. Wu, D.M. York , P.A. Kollman, AMBER 2015, (2015) University of California, San Francisco.
[22] N.J. Baxter, M.P. Williamson, Temperature dependence of 1H chemical shifts in proteins, J. Biomol. NMR, 9 (1997) 359-369.
[23] A.M. Finch, A.K. Wong, N.J. Paczkowski, S.K. Wadi, D.J. Craik, D.P. Fairlie, S.M. Taylor, Low-molecular-weight peptidic and cyclic antagonists of the receptor for the complement factor C5a, J. Med. Chem. 42 (1999) 1965-1974.
[24] T. Cierpicki, J. Otlewski, Amide proton temperature coefficients as hydrogen bond indicators in proteins, J. Biomol. NMR, 21 (2001) 249-261.
[25] MacroModel, version 9.9, Schrödinger, LLC, New York, NY, 2011.
[26] The PyMOL Molecular Graphics System, v1.6-alpha; Schrodinger LLC, New York, NY, 2013.
[27] A. Ganguly, B.K. Paul, S. Ghosh, S. Dalapati, N. Guchhait, Interaction of a potential chloride channel blocker with a model transport protein: a spectroscopic and molecular docking investigation, Phys. Chem. Chem. Phys. 16 (2014) 8465-8475.
[28] C. Hetenyi, D. van der Spoel, Blind docking of drug-sized compounds to proteins with up to a thousand residues, FEBS Lett. 580 (2006) 1447-1450.
[29] T. Aita, K. Nishigaki, Y. Husimi, Toward the fast blind docking of a peptide to a target protein by using a four-body statistical pseudo-potential, Computational biology and chemistry, 34 (2010) 53-62.
[30] C. Hetenyi, D. van der Spoel, Efficient docking of peptides to proteins without prior knowledge of the binding site, Protein Sci. 11 (2002) 1729-1737.
[31] M. Kovacs, J. Toth, C. Hetenyi, A. Malnasi-Csizmadia, J.R. Sellers, Mechanism of blebbistatin inhibition of myosin II, J. Biol. Chem. 279 (2004) 35557-35563.
[32] G.M. Morris, R. Huey, W. Lindstrom, M.F. Sanner, R.K. Belew, D.S. Goodsell, A.J. Olson, AutoDock4 and AutoDockTools4: Automated docking with selective receptor flexibility, J. Comput. Chem. 30 (2009) 2785-2791.
[33] G. Jones, P. Willett, R.C. Glen, Molecular recognition of receptor sites using a genetic algorithm with a description of desolvation, J. Mol. Biol. 245 (1995) 43-53.
[34] G. Jones, P. Willett, R.C. Glen, A.R. Leach, R. Taylor, Development and validation of a genetic algorithm for flexible docking, J. Mol. Biol. 267 (1997) 727-748.
[35] S. Gemma, C. Camodeca, M. Brindisi, S. Brogi, G. Kukreja, S. Kunjir, E. Gabellieri, L. Lucantoni, A. Habluetzel, D. Taramelli, N. Basilico, R. Gualdani, F. Tadini-Buoninsegni, G. Bartolommei, M.R. Moncelli, R.E. Martin, R.L. Summers, S. Lamponi, L. Savini, I. Fiorini, M. Valoti, E. Novellino, G. Campiani, S. Butini, Mimicking the intramolecular hydrogen bond: synthesis, biological evaluation, and molecular modeling of benzoxazines and quinazolines as potential antimalarial agents, J. Med. Chem. 55 (2012) 10387-10404.
[36] Prime, version 3.0, Schrödinger, LLC, New York, NY, 2011.
[37] Maestro, version 9.2, Schrödinger, LLC, New York, NY, 2011.
[38] M. Brindisi, S. Gemma, S. Kunjir, L. Di Cerbo, S. Brogi, S. Parapini, S. D'Alessandro, D. Taramelli, A. Habluetzel, S. Tapanelli, S. Lamponi, E. Novellino, G. Campiani, S. Butini, Synthetic spirocyclic endoperoxides: new antimalarial scaffolds, Med. Chem. Commun. 6 (2015) 357-362.

[39] M. Brindisi, S. Butini, S. Franceschini, S. Brogi, F. Trotta, S. Ros, A. Cagnotto, M. Salmona, A. Casagni, M. Andreassi, S. Saponara, B. Gorelli, P. Weikop, J.D. Mikkelsen, J. Scheel-Kruger, K. Sandager-Nielsen, E. Novellino, G. Campiani, S. Gemma, Targeting Dopamine D3 and Serotonin 5-HT1A and 5-HT2A Receptors for Developing Effective Antipsychotics: Synthesis, Biological Characterization, and Behavioral Studies, J. Med. Chem. 57 (2014) 9578-9597.
[40] S. Brogi, S. Butini, S. Maramai, R. Colombo, L. Verga, C. Lanni, E. De Lorenzi, S. Lamponi, M. Andreassi, M. Bartolini, V. Andrisano, E. Novellino, G. Campiani, M. Brindisi, S. Gemma, Disease-modifying anti-Alzheimer's drugs: inhibitors of human cholinesterases interfering with beta-amyloid aggregation, CNS Neurosci. Ther. 20 (2014) 624-632.
[41] M. Brindisi, S. Brogi, N. Relitti, A. Vallone, S. Butini, S. Gemma, E. Novellino, G. Colotti, G. Angiulli, F. Di Chiaro, A. Fiorillo, A. Ilari, G. Campiani, Structure-based discovery of the first non-covalent inhibitors of Leishmania major tryparedoxin peroxidase by high throughput docking, Sci. Rep. 5 (2015) 9705.
[42] M.Y. Wu, G. Esteban, S. Brogi, M. Shionoya, L. Wang, G. Campiani, M. Unzeta, T. Inokuchi, S. Butini, J. Marco-Contelles, Donepezil-like multifunctional agents: Design, synthesis, molecular modeling and biological evaluation, Eur. J. Med. Chem. (2015), doi.org/10.1016/j.ejmech.2015.10.001.
[43] S. Giovani, M. Penzo, S. Brogi, M. Brindisi, S. Gemma, E. Novellino, L. Savini, M.J. Blackman, G. Campiani, S. Butini, Rational design of the first difluorostatone-based PfSUB1 inhibitors, Bioorg. Med. Chem. Lett. 24 (2014) 3582-3586.
[44] S. Giovani, M. Penzo, S. Butini, M. Brindisi, S. Gemma, E. Novellino, G. Campiani, M.J. Blackman, S. Brogi, Plasmodium falciparum subtilisin-like protease 1: discovery of potent difluorostatone-based inhibitors, Rsc Adv. 5 (2015) 22431-22448.
[45] C.M. Henry, E. Hollville, S.J. Martin, Measuring apoptosis by microscopy and flow cytometry, Methods, 61 (2013) 90-97.
[46] C. Ulivieri, Cell death: insights into the ultrastructure of mitochondria, Tissue and Cell, 42 (2010) 339-347.
[47] J.K. Brunelle, A. Letai, Control of mitochondrial apoptosis by the Bcl-2 family, J. Cell Sci. 122 (2009) 437-441.
[48] S. Cory, J.M. Adams, The Bcl2 family: regulators of the cellular life-or-death switch, Nat. Rev. Cancer, 2 (2002) 647-656.
[49] E. Reits, A. Griekspoor, J. Neijssen, T. Groothuis, K. Jalink, P. van Veelen, H. Janssen, J. Calafat, J.W. Drijfhout, J. Neefjes, Peptide diffusion, protection, and degradation in nuclear and cytoplasmic compartments before antigen presentation by MHC class I, Immunity, 18 (2003) 97-108.
[50] B.A. Borgias, T.L. James, Mardigras - a Procedure for Matrix Analysis of Relaxation for Discerning Geometry of an Aqueous Structure, J. Magn. Reson. 87 (1990) 475-487.
[51] K. Lindorff-Larsen, S. Piana, K. Palmo, P. Maragakis, J.L. Klepeis, R.O. Dror, D.E. Shaw, Improved side-chain torsion potentials for the Amber ff99SB protein force field, Proteins, 78 (2010) 1950-1958.
[52] W.L. Jorgensen, D.S. Maxwell, J. TiradoRives, Development and testing of the OPLS all atom force field on conformational energetics and properties of organic liquids J. Am. Chem. Soc. 118 (1996) 11225-11236.
[53] W.C. Still, A. Tempczyk, R.C. Hawley, T. Hendrickson, Semianalytical Treatment of Solvation for Molecular Mechanics and Dynamics, J. Am. Chem. Soc. 112 (1990) 6127-6129.
[54] E. Polak, G. Ribiere, Note sur la convergence de directions conjuguées Rev. Fr. Inform. Rech. Operation., 3e Année, 16 (1969) 35-37.
[55] LigPrep, version 2.5, Schrödinger, LLC, New York, NY, 2011.

[56] J. Lowe, H. Li, K.H. Downing, E. Nogales, Refined structure of alpha beta-tubulin at 3.5 A resolution, J. Mol. Biol. 313 (2001) 1045-1057.
[57] Prime, version 3.0, Schrödinger, LLC, New York, NY, 2011.

Highlights

- Development of pro-apoptotic cyclic peptides and peptidomimetics
- Flow cytometry analysis on different tumor cell lines
- Confocal microscopy and cell lysates analyses to assess cell permeability
- Peptides and peptidomimetics conformational analysis by NMR
- β-tubulin staining to analyze the effect of the cyclic peptides on microtubules